SUPPORTING INFORMATION

The hereditary spastic paraplegia-related enzyme DDHD2 is a principal brain triglyceride lipase

Jordon Inloes, Ku-Lung Hsu, Melissa M. Dix, Andreu Viader, Kim Masuda, Thais Takei, Malcolm R. Wood, and Benjamin F. Cravatt

SI MATERIALS AND METHODS

Materials. Triazole urea compounds were synthesized in the laboratory following previously described procedures (1). Fluorophosphonate (FP)-rhodamine and FP-biotin were synthesized according to a previously described protocol (2-4). All deuterated lipid standards and substrates were purchased from Cayman Chemicals, Nu-Chek Prep, or Avanti Polar Lipids. Full-length cDNA encoding DDHD2 was purchased from Open Biosystems. All pharmacological studies were conducted in C57BL/6 mice unless otherwise indicated.

Generation of DDHD2$^{-/-}$ mice. The DDHD domain containing 2 (DDHD2)-targeting construct was generated by amplifying 5- and 3-kb regions of the *Ddhd2* gene adjacent to exon 8 (containing the catalytic serine 351) from a BAC clone containing the *Ddhd2* locus (clone RP24-277B3 from BACPAC Resources Center at Children's Hospital Oakland Research Institute) and sub-cloning these homologous arms into the NotI/SacII and XhoI/KpnI sites of the pKO-NTKV vector. The targeting construct was designed to replace exon 8 of the *Ddhd2* gene with a neomycin selection cassette upon homologous recombination. The targeting construct was electroporated into C57BL/6 Bruce 4-derived murine embryonic stem (ES) cells and screened for homologous recombination by Southern blot analysis with external probes located 5' and 3' of the targeted region. The 5' probe gave differential band sizes in WT (7.6 kb) or targeted (11 kb) genomic DNA digested with EcoRI. The 3' probe resulted in band sizes of 60.5 kb or 8.4 kb for XhoI-digested WT or targeted genomic DNA, respectively. One homologous recombinant, 127, was identified expanded and injected into albino C57BL/6 blastocysts. Blastocysts were implanted into pseudopregnant albino C57BL/6 females generate chimeric males. Several chimeras produced germ-line transmission of the targeted mutation, which was

confirmed by Southern analysis. PCR genotyping of genomic tail DNA was performed using the primers 5' GACCTTGTGTTCAGTCCTCAGCTCT-3', 5'-ACCCATGCACTGTAACTCTGATCC-3', and 5'-TAAAGCGCATGCTCCAGACTGCC-3', which amplify a 439- and 221-bp product from WT and targeted alleles, respectively.

Gene expression analysis of DDHD2. RNA was prepared using the RNeasy Midi Kit (Qiagen) from 50 mg of brain from *Ddhd2*$^{+/+}$ and *Ddhd2*$^{-/-}$ mice according to the manufacturer's instructions. A cDNA library was synthesized from extracted RNA with the Thermoscript RT-PCR system (Life Technologies) using oligo$(dT)_{20}$ primers. 1 µl of cDNA was used as template in a PCR reaction with 35 amplification cycles. DNA was melted for 15 s at 95°, primers annealed for 30 s at 60°, Taq polymerase extended the following primers for 60 s at 68°: DDHD2 Forward: 5'-GAGCGGATGCGGTATGCTGT-3' DDHD2 Reverse: 5'-AGTCTGACAGTAGGTGGGGCT-3' (Predicted product 672 bp). GAPDH Forward: 5'-TGTCTTCACCACCATGGAGAAGGC-3' GAPDH Reverse: 5'-TGGCAGTGATGGCATGGAACTGTGG-3' (Predicted product 252 bp). Products were visualized on a 2% agarose gel.

Primary neuron, astrocyte, and microglia cultures. The primary cell culture protocols used in this study were approved by the Scripps Research Institute Institutional Animal Care and Use Committee. Cortico-hippocampal neurons were prepared from embryonic day 18 C57BL/6 mice. Cortices/hippocampi were dissected, freed of meninges, and dissociated by incubation in Papain/DNase for 20 minutes at 37 °C followed by trituration. Dissociated cortico-hippocampal neurons were then washed with DMEM media supplemented with 10% FBS and 2 mM glutamine, prior to seeding them onto poly-D-lysine coated 10 cm culture dishes in neurobasal medium containing 2% B27 supplement, 2 mM glutamine, and 5 µM 5-fluoro-2′-deoxyuridine at a density of 8 x 10^6

cells/dish. A third of the media was exchanged twice per week. Neurons were harvested for proteome isolation after 16 days *in vitro*, at which point cultures contained <3% of non-neuronal cells.

Microglia were derived from mixed glial cultures prepared from postnatal day 2-3 C57BL/6 mouse forebrains. Briefly, forebrains were dissected, stripped of meninges, and digested in papain/DNAse (20 minutes at 37 °C) followed by 0.25% trypsin (15 minutes at 37 °C) and trituration. Dissociated cells were then cultured for 10 days in poly-D-lysine coated T75 tissue culture flasks in DMEM media supplemented with 10% FBS and 2 mM glutamine. After establishment of the astrocyte monolayer, the flasks were shaken for 2 h at 180 rpm to obtain the loosely attached microglia. Microglia were subsequently plated onto 10 cm dishes at a density of 3×10^6 cells/dish in Macrophage-SFM media (Gibco) supplemented with 1% FBS and 0.5 ng/ml of granulocyte macrophage-colony stimulating factor. The purity of these microglia cultures was >99%, and cells were allowed to sit for at least 72 h prior to harvesting them for proteome isolation.

Following isolation of microglia, established mixed glial cultures were treated with 8 μM cytosine-arabinoside for 3-5 days to kill actively dividing cells (e.g. microglia, fibroblast), and generate an astrocyte monolayer with >85% purity. These astrocytes were subsequently plated onto poly-D-lysine coated 10 cm dishes in DMEM media supplemented with 10% FBS and 2 mM glutamine, and allowed to become confluent. Upon reaching confluence, astrocytes were harvested for subsequent proteome isolation.

Behavioral analysis. All the behavioral tests were performed in The Scripps Research Institute mouse behavior assessment core facility. Mice were housed in groups in a temperature-controlled room with lights regulated on a 12-hr light/dark cycle (lights off at

0600 hours) and food and water were available ad libitum. Behavior was monitored during the dark phase when mice are most active. For our studies, a cohort of age- and sex-matched DDHD2$^{-/-}$, DDHD2$^{+/-}$, and DDHD2$^{+/+}$ mice from DDHD2$^{+/-}$ parents (n = 13 mice per genotype, mixed sex) were tested for locomotor activity and cognition at 6 months of age. Animal experiments were conducted in accordance with the guidelines of the Institutional Animal Care and Use Committee of The Scripps Research Institute.

Locomotor activity. Locomotor activity was measured in polycarbonate cages (42 x 22 x 20 cm) placed into frames (25.5 x 47 cm) mounted with two levels of photocell beams at 2 and 7 cm above the bottom of the cage (San Diego Instruments, San Diego, CA). These two sets of beams allowed for the recording of both horizontal (locomotion) and vertical (rearing) behavior. A thin layer of bedding material was applied to the bottom of the cage. Mice were tested for 120 min and data were collected in 5 min intervals.

Rotarod test. Rotarod balancing requires a variety of proprioceptive, vestibular, and fine-tuned motor abilities as well as motor learning capabilities (5). A Rotarod Series 8 apparatus (IITC Life Sciences, Woodland Hills, CA) was used and both accelerating and constant speed tests were performed. When an animal dropped onto the individual sensing platforms below the rotating rod, test results were recorded. For initial training, an accelerating test strategy was used whereby the rod started at 0 rpm and then accelerated at 10 rpm min^{-1}. The mice were tested 6 times per day in two sets of 3 trials; with 1 min between each trial within a set and approximately 1 h between each set. This was repeated for two days. One week later, the mice were retested under the same conditions in one set of 3 trials in order to look at retention of motor memory.

Twelve weeks later the mice were examined in two additional rotarod tests designed to be more challenging than the training protocol. First, mice were tested in one set of 3 trials on the accelerating rotarod, this time at 20 rpm min^{-1}. Finally, the mice

were run in a constant 12 rpm test to examine the length of time the mouse would remain on the bar as an estimation of fatigue.

Footprint pattern test. Basic gait measures can be assessed using simple footprint pattern analysis (5, 6). For example, a mouse model of Ataxia telangiectasia had shorter stride lengths than WT mice (7). Non-toxic paint was applied to each mouse's paws (a different color was used for front and back paws). The mouse was then placed at one end of a runway covered in paper and allowed to ambulate until their paws no longer left marks. Measurements were forelimb and hindlimb stride lengths (left and right). Three full strides were averaged for each mouse's values. Data were excluded from mice that did not make 3 measurable strides (i.e. they circled or stopped).

Optomotor test of vision. To test visual ability we measured tracking of a moving object as described previously (8). This test utilizes a stationary elevated platform surrounded by a drum with black and white striped walls. The mouse is placed on the platform to habituate for 1 min and then the drum is rotated at 2 rpm in one direction for 1 min, stopped for 30 s, and then rotated in the other direction for 1 min. The total number of head tracks (15 degree movements at the speed of the drum) is recorded. Mice with intact vision track 5-12 times, whereas blind mice do not track at all.

Y-maze test for spontaneous alternations. To determine spontaneous alternation behavior, a measure of spatial working memory, exploratory behavior and responsiveness to novelty (9, 10), we tested mice in a Y-maze with 34 x 8 x 14 cm arms. Each mouse received one 5 min trial during which arm choices and total numbers of arm entries were recorded. Spontaneous alternation, expressed as percentage, refers to the ratio of arm choices differing from the previous two choices, to the total number of arm entries. Mice have the opportunity to do repeated entries into a single arm, resulting in a chance performance level of 22% (2/9) for spontaneous alternations (11, 12). Healthy

young mice make 60-70% spontaneous alternations. In the TSRI MBAC we have observed 6-month old APP-Swe transgenic mice to make 50% spontaneous alternations relative to 63% in age and litter-matched wild type mice (alpha < 0.05, beta = 0.8, delta = 30%, within-group variance < 10%). This is consistent with the literature using the same test at the same age (13).

Barnes maze test. The Barnes maze is a spatial learning and memory test (14) sensitive to impaired hippocampal function (15). This task has the benefit of minimizing pain and distress to the animal. Traditional spatial tests involve swimming in opaque water to locate a hidden platform (the Morris water maze). The Barnes maze is less physically taxing than the Morris water maze, making it more suitable for mice which are not as strong as rats, and also suitable for studies in all ages and abilities of mice (16). In addition, the strategies used by the animals to perform the task are readily revealed. The Barnes maze used was an opaque Plexiglas disc 75 cm in diameter elevated 58 cm above the floor by a tripod. Twenty holes, 5 cm in diameter, were located 5 cm from the perimeter, and a black Plexiglas escape box (19 x 8 x 7 cm) was placed under one of the holes. Distinct spatial cues were located all around the maze and were kept constant throughout the study.

On the first day of testing, a training session was performed, which consisted of placing the mouse in the escape box and leaving it there for one minute. One minute later, the first session was started. At the beginning of each session, the mouse was placed in the middle of the maze in a 10 cm high cone-shaped silver start chamber. After 10 sec the start chamber was removed, a buzzer (80 dB) and a light (400 lux) were turned on, and the mouse was set free to explore the maze. The session ended when the mouse entered the escape box or after 3 min elapsed. When the mouse entered the escape tunnel, the buzzer was turned off and the mouse was allowed to remain in the dark for one minute. If the mouse did not enter the box by itself it was gently put in the

escape box for one minute. The tunnel was always located underneath the same hole (stable within the spatial environment), which was randomly determined for each mouse. Mice were tested once a day for 4 days for the acquisition portion of the study.
A probe test was performed on the day following the final acquisition trial. For the probe tests, the escape box was removed and the mouse was allowed to freely explore the maze for 3 min. The time spent in each quadrant was determined and the percent time spent in the target quadrant (the one originally containing the escape box) was compared with the average percent time in the other three quadrants. This is a direct test of spatial memory as there is no potential for local cues to be used in the mouse's behavioral decision.

Finally, 2 weeks following the probe test, the mice were tested again with the escape box in the original position (retention test). This allows for the examination of long-term memory. Each session was videotaped and scored by an experimenter blind to the genotype of the mouse. Measures recorded included the latency to escape the maze and percent of time spent in each quadrant.

Untargeted metabolomics analysis by LC-MS. We performed untargeted metabolomics experiments as previously described (17, 18). Age-matched (2-month old) *Ddhd2*$^{-/-}$ and *Ddhd2*$^{+/+}$ males were anesthetized with isofluorane and sacrificed by decapitation. Brains were harvested, laterally sectioned, and immediately snap frozen in liquid N_2. A frozen brain hemisphere was weighed and subsequently Dounce homogenized in 2:1:1 (v/v/v) $CHCl_3$:MeOH:PBS (8 mL) containing 1 nmol of C:15 monoacylglycerol (MAG) and PDA added as internal standards for positive- and negative-mode analysis, respectively. The mixture was then vortexed and centrifuged at 1,400 x g for 3 min. The organic fraction was carefully removed and $CHCl_3$ was added until the final volume was again 8 mL and the extraction was repeated. The organic

fractions were then combined and dried under a N2 stream and lipids resolubilized in 2:1 (v/v) $CHCl_3$:MeOH (120 µL) and 20 µL was injected onto an Agilent 6520 Q-TOF mass spectrometer (MS) instrument. Liquid chromatography (LC) separation was achieved using a Gemini reverse-phase C18 column (50 x 4.6 mm with 5 µm diameter particles, Phenomonex) along with a pre-column (C18, 3.5 µm, 2 mm x 20 mm). For analysis of triacylglycerols (TAGs) a Luna C5 column (50 x 4.60 mm with 5 µm diameter particles) or Poroshell C18 column (75 x 1.0mm with 2.7 µm diameter particles) from Agilent was used. Mobile phase A was made of 95:5 (v/v) H_2O:MeOH, and mobile phase B was composed of 60:35:5 (v/v/v) *i*-PrOH:MeOH:H_2O. Ammonium hydroxide (0.1%) and formic acid (0.1%) was included to assist in ion formation in negative and positive ionization modes, respectively. For analysis of TAGs, 10 mM ammonium formate was also used in addition to 0.1% formic acid to assist in positive ionization and NH_4+ adduct formation. MS analysis was performed with an ESI source in scanning mode from *m/z* = 50 – 1,200, capillary voltage set to 4.0 kV, and the fragmentor voltage set to 100 V. The drying gas temperature was set to 350 °C, drying gas flow rate was 11 L/min, and nebulizer pressure was 45 psi. LC-MS data was analyzed by XCMS (available for free at http://metlin.scripps.edu/xcms) (19). The XCMS software package automatically identifies, matches, aligns, and integrates chromatographic peaks corresponding to metabolites and identifies *m/z* values that are significantly altered between sample groups. DMP results from two independent biological replicates were compared and filtered for *m/z* values that appeared in both datasets with >2-fold change between genotypes, >10,000 average peak-integration area, and $p < 0.05$. Results from our studies are presented as fold-change of average integrated ion intensities measured in DDHD2$^{-/-}$ versus DDHD2$^{+/+}$ brain metabolomes. We determined molecular identity of altered metabolites by searching experimental *m/z* values against known metabolites in

Metlin (http://metlin.scripps.edu/metabo_search_alt2.php) and the Lipid Maps Structure Database (www.lipidmaps.org/data/structure/index.html). Structural assignments were confirmed by co-elution with commercially available standards and/or fragmentation analysis as described below.

Structural assignment by LC-MS/MS. Fragmentation analysis was performed on an Agilent 6520 or Agilent 6538 Q-TOF MS with an ESI source, using LC conditions described above for untargeted metabolomics analysis in positive ionization mode using the Luna C5 column or Poroshell C18 column in the presence of 10 mM ammonium formate. The *m/z* values corresponding to endogenous metabolites or parent ions of synthetic standards [$(M+NH4)^+$] were targeted for MS/MS analysis, and MS1 and MS2 spectra were acquired at a rate of 1.02 spectra per second.

Targeted LC-MS metabolite measurements. We measured tissue TAG levels in $DDHD2^{-/-}$ and $DDHD2^{+/+}$ age- and sex-matched mice by multiple reaction monitoring (MRM) methods as previously described (20, 21) (N = 5 – 9 per genotype). To measure age-dependent alterations in TAGs, we performed lipid measurements on mice from different age groups: 3 weeks, 3 months, and 6-10 month old mice. MS parameters used to measure MAGs, DAGs, and TAGs by MRM analysis are listed in **Table S2**. Tissue metabolomes were prepared as described above for untargeted metabolomics analysis except C17:1 or C17:0/C17:1/C17:0-d5 TAG lipids were added as internal standards. Tissue metabolomes (10 µL) were injected onto a Luna C5 column in tandem with either a 6410B or 6460 triple quadrupole (QQQ)-MS instrument using mobile phases described above for TAG analysis and the following method: 0.1 mL/min 0% buffer B for 5 min, 0.4 mL/min linear gradient from 30 to 100% buffer B over 15 min, 0.5 mL/min 100% buffer B for 8 min, and 0.5 mL 0% buffer B for 3 min (total run time of 31 min per sample). MS

analysis was performed by targeted MRM with an ESI source in positive-ion mode for MAGs, DAGs, and TAGs using the precursor to product ion transition and collision energies shown in **Table S2**. Dwell times for each lipid were set to 100 ms, and the following MS parameters were used for the 6410B QQQ: capillary voltage = 3.5 kV, drying gas temperature = 250 °C, drying gas flow rate = 9 L/min, and nebulizer pressure = 35 psi. For the 6460 QQQ, the following MS parameters were used: capillary voltage = 3.5 kV, drying gas temperature = 250 °C, drying gas flow rate = 9 L/min, and nebulizer pressure = 35 psi, sheath gas temperature = 375 °C, and sheath gas flow rate = 10 L/min. Endogenous lipids were quantified by measuring the area under the peak in comparison with the appropriate unnatural internal standard and normalizing for tissue weight.

Electron and light microscopy analysis. Mice were exsanguinated by perfusion with saline followed by a mixture of 4% paraformaldehyde, 1.5% glutaraldehyde in 0.1M Na cacodylate buffer (pH 7.3). Following dissection of the whole brain, fixation continued overnight in the same fixative. Thick sagittal slices were taken bilateral to the midline with a single edged razor blade and the slices washed overnight in cacodylate buffer. Each thick slice was further trimmed specifically to two regions of interest (ROI) for subsequent processing. Each ROI was incubated in 2% osmium tetroxide for 3 h, buffer washed and dehydrated in graded ethanol series before being transitioned in propylene oxide and flat embedded in EMbed 812 / Araldite (Electron Microscopy Sciences, Hatfield PA). Thick sections (2 μm) were cut, mounted on glass slides and stained in toluidine blue. Thick sections were mounted and cover slipped before scanning with a Leica SCN400 slide scanner (Buffalo Grove IL). Composite 40x images were stitched in Adobe Photoshop (San Jose CA). Image Pro Plus 7.0 (Media Cybernetics, Rockville MD) was used to extract the blue color channel of each image for thresholding and

particle measurement. Intensity thresholds were set at: >50, <120, and particles were detected with the following parameters: area(pixels): >2; aspect ratio: >1,<2.5; roundness: >0,<4.5. Subsequently, 70 nm thin transverse sections were cut with a diamond knife (Diatome, Electron Microscopy Sciences, Hatfield PA), mounted on copper slot grids coated with parlodion and stained with uranyl acetate and lead citrate for examination on a Philips CM100 electron microscope (FEI, Hillsbrough OR). Images were documented using a Megaview III ccd camera (Olympus Soft Imaging Solutions GmbH, Münster, Germany) for subsequent handling in Adobe Photoshop.

Preparation of tissue proteomes. Mouse tissues were homogenized in cold PBS, pH 7.5, in a bullet blender (Next Advance, Inc.) per the manufacturer's instructions followed by a low-speed spin (1,400 x g, 5 min) to remove debris. The membrane and cytosolic fractions were separated by ultracentrifugation (100,000 x *g*, 45 min) of the resulting homogenate lysate. Afterward removal of the soluble supernatant, the membrane pellet was washed 1X with cold PBS followed by resuspension in cold PBS buffer by sonication. Total protein concentration in membrane and soluble fractions were determined using the Bio-Rad DC protein assay kit. Samples were stored at -80 °C until further use.

Cell and Tissue Profiling by Gel-based Competitive ABPP. Gel-based ABPP assays were performed as previously reported (22). Cell or tissue proteomes were treated with either FP-rhodamine or HT-01 (1 μM final concentration) in a 50 μL total sample volume. For HT-01 labeled samples, 2 mg/mL of proteome was used to enhance endogenous DDHD2 signals; 1 mg/ml proteome was used for labeling with the broad-spectrum serine hydrolase probe FP-Rh. Probe labeling was carried out for 30 min at 37 °C followed by addition of 16.7 μL of 4X SDS-PAGE loading buffer to quench the reaction. After

separation by SDS-PAGE (10% acrylamide), samples were visualized by in-gel fluorescence scanning using a flatbed fluorescence scanner (Hitachi FMBio IIe).

***In situ* studies with KLH45 and KLH40**. Neuro2A cells passaged in Light or Heavy ([$^{13}C_6{}^{15}N_4$]-L-Arginine, [$^{13}C_6{}^{15}N_2$]-L-Lysine) SILAC DMEM medium were treated with DMSO or test compound (25 nM KLH45 or KLH40), respectively, for 4 hr at 37 °C. Cells were subsequently washed with PBS (2X), harvested, and prepared for SILAC analysis as described below.

ABPP-SILAC sample preparation and analysis. ABPP-SILAC analysis was carried out as previously reported(1, 23). In brief, Neuro2A cells grown for 10 passages in either light or heavy SILAC DMEM medium supplemented with 10% (v/v) dialyzed FCS and 2 mM-L-glutamine. Light medium was supplemented with 100 µg/mL L-arginine and 100 µg/mL L-lysine. Heavy medium was supplemented with 100 µg/mL [$^{13}C_6{}^{15}N_4$]-L-Arginine and 100 µg/mL [$^{13}C_6{}^{15}N_2$]-L-Lysine. Heavy cells were treated with test compound, and light cells were treated with DMSO for 4 h at 37 °C. Cells were washed with 2X with PBS, and proteomes processed for ABPP analysis as described above. Membrane and Soluble proteomes were prepared for multidimensional liquid chromatography tandem mass spectrometry (MudPIT) analysis as previously described (23).

Tissue preparation for ABPP-reductive dimethylation. Mouse half brains were homogenized in PBS using a bullet blender. Homogenates were then subjected to centrifugation at 100,000 g to separate membrane and soluble fractions. ABPP experiments were performed as previously described (23), with minor adjustments. The last wash steps and trypsin digestion were performed in 100 mM triethylammonium bicarbonate buffer in preparation for downstream reductive dimethylation labeling.

Reductive dimethylation was performed as previously described (24). Briefly, either 4% C13 –labeled deuterated formaldehyde (heavy) or formaldehyde (light) was added to a final concentration of 0.15%, followed by addition of sodium cyanoborohydride to a final concentration of 22.2 mM. Following a 1 h incubation period at room temperature, the reaction was quenched by addition of 1% ammonium hydroxide and 5% formic acid to final concentrations of 0.23% and 0.5%, respectively. The samples were then combined and analyzed on a Velos-Orbitrap mass spectrometer.

Mass spectrometry and data analysis. Mass spectrometry was performed using a Thermo Orbitrap Velos mass spectrometer, using a previously described protocol (25, 26). Peptides were eluted using a five-step multidimensional LC-MS [MudPIT (27)] protocol (using 0%, 25%, 50%, 80% and 100% salt bumps of 500 mM aqueous ammonium acetate, followed by an increasing gradient of aqueous acetonitrile and 0.1% formic acid in each step), and data were collected in data-dependent acquisition mode [400–1800 mass to charge ratio (*m/z*) and 30 data-dependent fragmentation (MS2) scans] with dynamic exclusion enabled (repeat count of 1, exclusion duration of 20 s). Prolucid searches allowed for static modification of cysteine residues (+57.0215 *m/z*; iodoacetamide alkylation) and required peptides to contain at least one tryptic end. For ReDiMe samples, each data set was independently searched with light and heavy parameter files; for the light search, static modifications on lysine (+ 28.0313 *m/z*) and N-termini (+ 28.0313 *m/z*) were specified; for the heavy search, static modifications on lysine (+ 34.06312 *m/z*) and N-termini (+ 34.06312 m/z) were specified. For SILAC samples, datasets were searched independently with the following parameter files; for the light search, all amino acids were left at default masses; for the heavy search, static modifications on lysine (+8.0142 *m/z*) and arginine (+10.0082 *m/z*) were specified. The precursor-ion mass tolerance was set to 50 ppm. The data were searched using a

mouse reverse-concatenated nonredundant (gene-centric) FASTA database that was assembled from the Uniprot database (http://www.uniprot.org/). The resulting matched MS2 spectra were assembled into protein identifications, then filtered using DTASelect (version 2.0.47). Peptides were restricted to a specified false positive rate of <0.5%. ReDiMe and SILAC ratios were quantified using in-house software as described [CIMAGE (28)]. Briefly, extracted MS1 ion chromatograms (± 10 ppm) from both 'light' and 'heavy' target peptide masses (*m/z*) were generated using a retention time window (± 10 min) centered on the time when the peptide ion was selected for MS/MS fragmentation, and subsequently identified. Next, the ratio of the peak areas under the light and heavy signals (signal-to-noise ratio > 2.5) are calculated. Computational filters used to ensure that the correct peak-pair is used for quantification include a co-elution correlation score filter ($R^2 \geq 0.8$), removing target peptides with bad co-elution profile, and an 'envelope correlation score' filter ($R^2 > 0.8$) that eliminates target peptides whose predicted pattern of the isotopic envelope distribution does not match the experimentally observed high-resolution MS1 spectrum. Also, peptides detected as singletons, where only the heavy or light isotopically labeled peptide was detected and sequenced, but which passed all other filtering parameters, were given a standard ratio of 20, which is the maximum ReDiMe or SILAC ratio reported here.

LC-MS TAG and DAG hydrolysis assay. DDHD2 proteins were recombinantly expressed as FLAG-tagged fusions in HEK293T cells by transient transfection as previously described (22). HEK293T-DDHD2 soluble lysates were diluted to 0.4 mg/mL in PBS (50 µL reaction volume). Lysates were then treated with DMSO or compound (2 µM final) for 30 min at 37 °C. The substrate was prepared by sonicating C18:1/C18:1/C18:1 TAG or C18:1/C18:1 DAG in assay buffer (25 mM HEPES, 150 mM NaCl, 2 mM EDTA, 0.1% n-Decyl-β-D-Maltopyranoside) and 100 µL of solubilized

substrate was added to the sample reaction (167 μM final concentration of TAG or DAG) and then incubated for 90 min at 37 °C. The reaction was quenched by adding 300 μL of 2:1 (v/v) $CHCl_3$:MeOH, doped with 100 pmol of C15:0 fatty acid standard, vortexed and then centrifuged (1,400 x *g*, 3 min) to separate the phases. The organic phase was subjected to LC-MS analysis by injecting 20 μl onto a Kinetix C18 column (50 x 4.60 mm with 2.6 μm diameter particles, Phenomenex) in tandem with the Agilent 6560 instrument using the following LC parameters: Mobile phase A was made of 5:1:4 (v/v/v) *i*-PrOH:MeOH:H_2O, and mobile phase B was composed of 99:1 (v/v) *i*-PrOH:H_2O. Acetic acid (0.1%) and ammonium acetate (5 mM) were included to assist in ion formation. For targeted analysis, the flow rate for each run started at 0.35 mL/min with 0% B. At 5 min, the solvent was changed to 20% B with a flow rate of 0.35 mL/min, 30% B at 25 min at 0.35 mL/min, 95% B at 35 min at 0.35 mL/min and held at 95% B for 1 min before equilibrating for 2 min at 0% B at 0.35 mL/min. MS parameters used in the analysis: capillary voltage = 3.5 kV, drying gas temperature = 300 °C, drying gas flow rate = 11 L/min, and nebulizer pressure = 35 psi, sheath gas temperature = 300 °C, and sheath gas flow rate = 11 L/min. Free fatty acid (C18:1) release was quantified by measuring the area under the peak in comparison with the C15:0 fatty acid internal standard.

Radiolabeled TLC TAG hydrolysis assay. TAG hydrolysis activity of DDHD2 was also assessed using a radiolabeled TLC assay (29). HEK293T-DDHD2 cell or mouse brain soluble lysates were diluted to 0.4 and 4 mg/mL, respectively, in PBS (50 μL reaction volume) and pretreated with DMSO or compound (2 μM final) for 30 min at 37 °C. A mixture of [carboxyl-^{14}C]-C18:1/C18:1/C18:1 TAG (^{14}C-triolein; PerkinElmer) and ^{12}C-triolein were sonicated in assay buffer and 100 μL of solubilized TAGs (final TAG concentration of 22 and 45 μM for ^{14}C- and ^{12}C-triolein, respectively) was added to samples and incubated for 90 min at 37 °C. Reactions were quenched by adding 600 μL

of 2:1 (v/v) $CHCl_3$:MeOH and 150 µL of assay buffer, vortexed for 15 sec, and centrifuged for 3 min at 1,400 x *g*. The organic phase was transferred to a new vial and extracted lipids dried under N_2 stream. Dried lipids were reconstituted in 15 µL of $CHCl_3$, separated by thin-layer chromatography (TLC) on precoated, glass backed silica gel 60 F_{254} plates using a previously described mobile phase (30) with the use of 3% acetic acid (93:4:3 $CHCl_3$, MeOH, AcOH) to minimize trailing of the free fatty acid spot. Formation of ^{14}C-DAG, ^{14}C-MAG, and ^{14}C-oleic acid was measured by autoradiography using the following R_f values for lipids species: TAG, 0.83; DAG, 0.49; FFA, 0.33; MAG, 0.16. Integrated intensity of spots corresponding to TAG, DAG, MAG and free fatty acid were measured with ImageJ software (http://imagej.nih.gov/ij/) and hydrolysis products were calculated as percent of non-hydrolyzed ^{14}C-TAG and normalized to mock-transfected or heat-denatured samples for cell lysates or brain lysates, respectively.

Determination of IC_{50} values. For gel-based competitive ABPP studies, the percentage of enzyme activity remaining was determined by measuring the integrated optical density of bands using ImageJ software. IC_{50} values were calculated by nonlinear regression analysis of dose-response curves generated using GraphPad Prism.

Statistical analysis. Data are shown as the mean $\pm$ s.e.m. A Student's t test (unpaired, two-tailed) was used to determine differences between two groups. A P value less than 0.05 was considered significant. All statistical analyses were conducted using GraphPad Prism. For multi-group comparisons, 2-way ANOVA (Fisher's LSD) were computed using a P-value threshold of 0.05.

General synthetic methods. Chemicals and reagents were purchased from Sigma-Aldrich, Acros, Matrix Scientific, Fisher, Combi-Blocks, Fluka, Maybridge, Aquila

Pharmatech, and BioBlocks and used without further purification unless noted otherwise. Dry solvents were obtained by passing commercially available pre-dried, oxygen-free formulations through activated alumina columns. Reactions were carried out under nitrogen atmosphere using oven-dried glassware except where noted. Flash chromatography was carried out using 230-400 mesh silica and reactions were monitored by analytical thin-layer chromatography (TLC) on precoated, glass backed silica gel 60 F_{254} plates. Reactions were purified either by preparative TLC or by flash chromatography on 40-60 MYM mesh silica gel. ^{1}H-NMR and spectra were recorded in $CDCl_3$ on a Bruker DRX-600 spectrometer and were referenced to trimethylsilane (TMS). Chemical shifts were reported in ppm relative to TMS and *J* values reported in Hz. High resolution mass spectrometry (HRMS) experiments were performed at The Scripps Research Institute Mass Spectrometry Core on an Agilent mass spectrometer using electrospray ionization-time of flight (ESI-TOF). Asterisk in the ^{1}H-NMR spectra designates the triazole ring proton. From previous studies (23), we have found this signal to be suppressed in all 1,4-regiosomeric triazole-urea compounds bearing a 2-benzyl (e.g. KT116, KT109, KT172) but not 2-phenyl (e.g. KT195) group.

Synthesis of *N*-cyclohexyl-*N*-phenethyl-4-(4-(trifluoromethoxy)phenyl)-2*H*-1,2,3-triazole-2-carboxamide. A solution of phenylethanamine (100 mg, 0.83 mmol) in THF (8.3 mL) was treated with cyclohexanone (73 mg, 0.74 mmol, 0.9 equiv) and $NaBH(OAc)_3$ (250 mg, 1.16 mmol, 1.4 equiv), and the mixture was stirred at room temperature for 2 hr or until the reaction was complete. The mixture was poured into H_2O and extracted with ethyl acetate. The organic layer was washed with H_2O and brine, dried over Na_2SO_4 and concentrated under reduced pressure. The residue was purified by silica gel chromatography (DCM/MeOH = 9:1) to afford *N*-phenethylcyclohexanamine. *N*-phenethylcyclohexanamine (50 mg, 0.24 mmol) was dissolved in THF (2 mL) and

treated with iPr_2NEt (0.13 mL, 0.72 mmol, 3.0 equiv) and triphosgene (36 mg, 0.12 mmol, 0.5 equiv) followed by stirring of the reaction mixture for 30 min at 4 °C. The mixture was poured into H_2O and extracted with ethyl acetate. The organic layer was washed with H_2O and brine, dried over Na_2SO_4 and concentrated under reduced pressure. The intermediate was dissolved in THF (5 mL) and iPr_2NEt (0.13 mL, 0.72 mmol, 3.0 equiv), DMAP (30 mg, 0.24 mmol, 1.0 equiv) and 4-(4-(trifluoromethoxy)phenyl)-1*H*-1,2,3-triazole (31) (56 mg, 0.24 mmol, 1.0 equiv) were added to the solution. The mixture was stirred for 2 hr at 60 °C and poured into saturated aqueous NH_4Cl solution. The mixture was extracted with ethyl acetate, washed with H_2O and brine, dried over Na_2SO_4 and concentrated under reduced pressure. pTLC (ethyl acetate:hexane = 1:4) afforded **KLH45** as a bottom spot of the triazole urea isomers (30% yield).

^{1}H NMR (600 MHz, $CDCl_3$) δ 8.07 (s, 1H), 7.93 – 7.89 (m, 2H), 7.48 – 6.93 (m, 7H), 4.22 – 3.72 (m, 1H), 3.67 – 3.59 (m, 2H), 3.19 – 2.78 (m, 2H), 2.02 – 1.05 (m, 10H).

HRMS calculated for $C_{24}H_{26}F_3N_4O_2$ [M+H]+ 459.2002, found 459.2004.

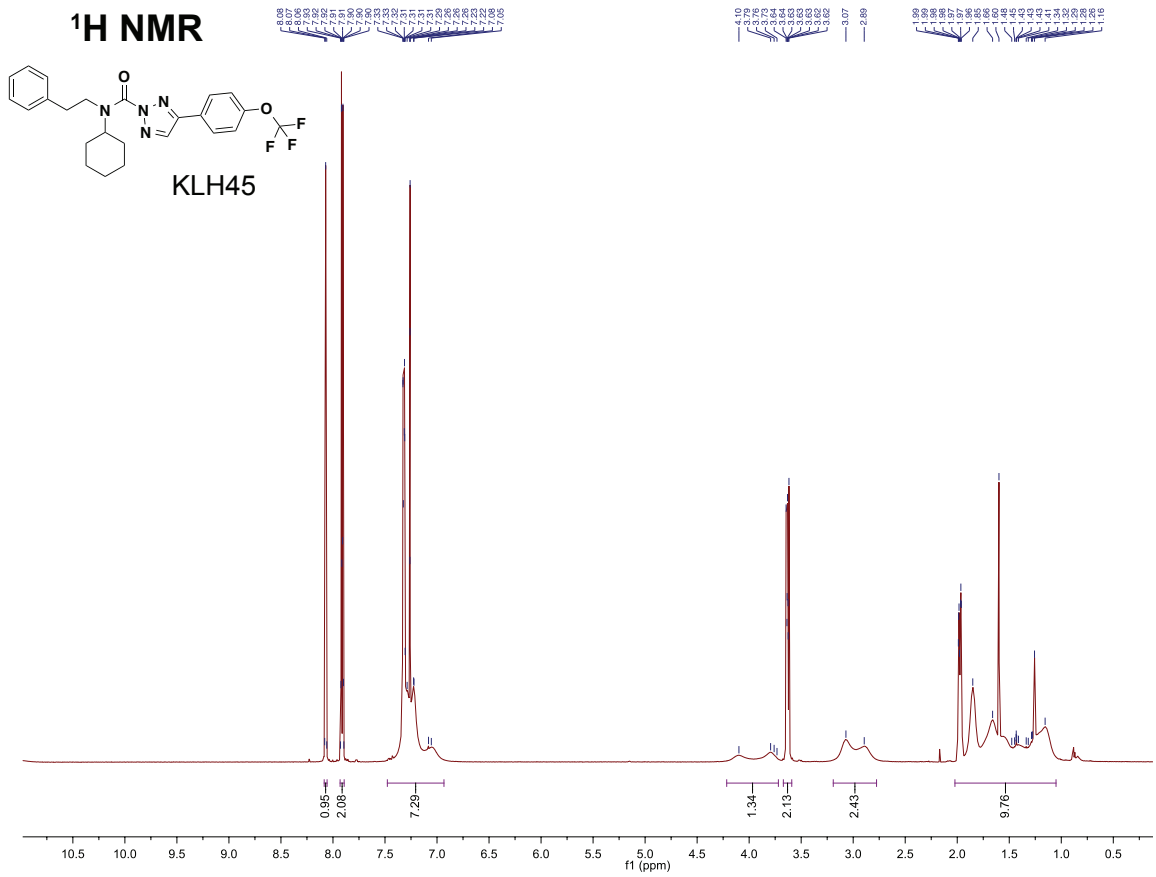

Synthesis of (*R*)-(3-benzylmorpholino)(4-(4-(trifluoromethoxy)phenyl)-1*H*-1,2,3-triazol-1-yl)methanone. A solution of (*R*)-3-benzylmorpholine (30 mg, 0.17 mmol) was dissolved in THF (2 mL) and treated with iPr_2NEt (0.09 mL, 0.51 mmol, 3.0 equiv) and triphosgene (25 mg, 0.09 mmol, 0.5 equiv) followed by stirring of the reaction mixture for 30 min at 4 °C. Next, the mixture was poured into H_2O and extracted with ethyl acetate. The organic layer was washed with H_2O and brine, dried over Na_2SO_4 and concentrated under reduced pressure. The intermediate was dissolved in THF (5 mL) and iPr_2NEt (0.09 mL, 0.51 mmol, 3.0 equiv), DMAP (21 mg, 0.17 mmol, 1.0 equiv) and 4-(4-(trifluoromethoxy)phenyl)-1*H*-1,2,3-triazole (31) (39 mg, 0.17 mmol, 1.0 equiv) were added to the solution. The mixture was stirred for 2 hr at 60 °C and poured into saturated aqueous NH_4Cl solution. The mixture was extracted with ethyl acetate, washed with H_2O and brine, dried over Na_2SO_4 and concentrated under reduced pressure. pTLC (ethyl

acetate:hexane = 1:4) afforded **KLH40** as a top spot of the triazole urea isomers (28% yield).

^{1}H NMR (600 MHz, $CDCl_3$) δ 7.81 (s, 2H), 7.54 – 6.96 (m, 7H), 5.05 – 4.34 (m, 1H), 4.23 – 3.57 (m, 6H), 3.47 – 2.77 (m, 2H). Asterisk in the ^{1}H-NMR spectrum designates the triazole ring proton. From previous studies (23), we have found this signal to be suppressed in all 1,4-regiosomeric triazole-urea compounds bearing a 2-benzyl (e.g. KT116, KT109, KT172) but not 2-phenyl (e.g. KT195) group. For KLH40, the triazole proton was observed with a chemical shift of 8.38 – 8.17.

HRMS calculated for $C_{21}H_{20}F_3N_4O_3$ [M+H]+ 433.1482, found 433.1484.

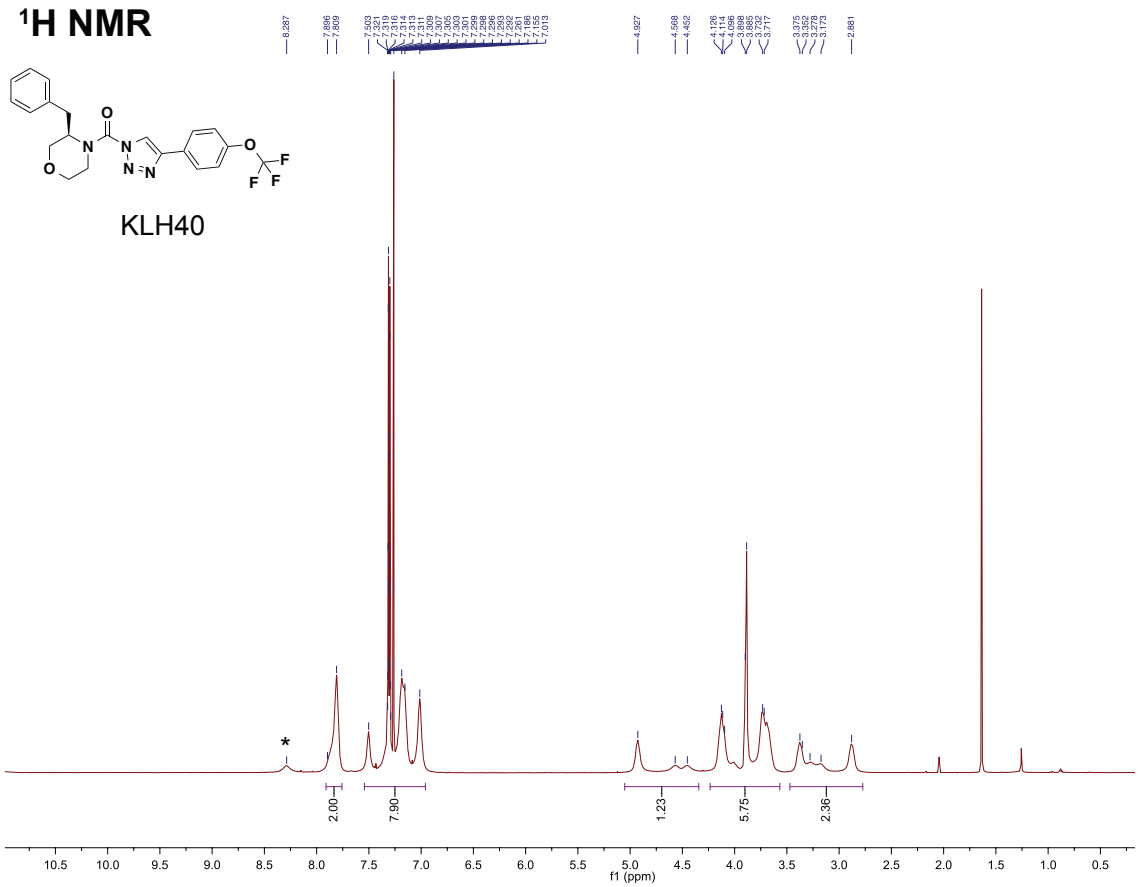

References.

1. Adibekian A*, et al.* (2011) Click-generated triazole ureas as ultrapotent in vivo-active serine hydrolase inhibitors. *Nat Chem Biol* 7(7):469-478.
2. Liu Y, Patricelli MP, & Cravatt BF (1999) Activity-based protein profiling: the serine hydrolases. *Proc. Natl. Acad. Sci. U.S.A.* 96:14694-14699.
3. Patricelli MP, Giang DK, Stamp LM, & Burbaum JJ (2001) Direct visualization of serine hydrolase activities in complex proteome using fluorescent active site-directed probes. *Proteomics* 1:1067-1071.
4. Kidd D, Liu Y, & Cravatt BF (2001) Profiling serine hydrolase activities in complex proteomes. *Biochemistry* 40:4005-4015.
5. Carter RJ, Morton J, & Dunnett SB (2001) Motor coordination and balance in rodents. *Current protocols in neuroscience / editorial board, Jacqueline N. Crawley ... [et al.]* Chapter 8:Unit 8 12.
6. Crawley JN & Paylor R (1997) A proposed test battery and constellations of specific behavioral paradigms to investigate the behavioral phenotypes of transgenic and knockout mice. *Hormones and behavior* 31(3):197-211.
7. Barlow C*, et al.* (1996) Atm-deficient mice: a paradigm of ataxia telangiectasia. *Cell* 86(1):159-171.
8. Amador-Arjona A*, et al.* (2011) Primary cilia regulate proliferation of amplifying progenitors in adult hippocampus: implications for learning and memory. *The Journal of neuroscience : the official journal of the Society for Neuroscience* 31(27):9933-9944.
9. Hughes RN (2004) The value of spontaneous alternation behavior (SAB) as a test of retention in pharmacological investigations of memory. *Neuroscience and biobehavioral reviews* 28(5):497-505.
10. Lalonde R (2002) The neurobiological basis of spontaneous alternation. *Neuroscience and biobehavioral reviews* 26(1):91-104.
11. Holcomb LA*, et al.* (1999) Behavioral changes in transgenic mice expressing both amyloid precursor protein and presenilin-1 mutations: lack of association with amyloid deposits. *Behavior genetics* 29(3):177-185.
12. Pennanen L, Wolfer DP, Nitsch RM, & Gotz J (2006) Impaired spatial reference memory and increased exploratory behavior in P301L tau transgenic mice. *Genes, brain, and behavior* 5(5):369-379.
13. Mitani Y*, et al.* (2012) Differential effects between gamma-secretase inhibitors and modulators on cognitive function in amyloid precursor protein-transgenic and nontransgenic mice. *The Journal of neuroscience : the official journal of the Society for Neuroscience* 32(6):2037-2050.
14. Barnes CA (1979) Memory deficits associated with senescence: a neurophysiological and behavioral study in the rat. *Journal of comparative and physiological psychology* 93(1):74-104.
15. Paylor R, Zhao Y, Libbey M, Westphal H, & Crawley JN (2001) Learning impairments and motor dysfunctions in adult Lhx5-deficient mice displaying hippocampal disorganization. *Physiology & behavior* 73(5):781-792.
16. Bach ME, Hawkins RD, Osman M, Kandel ER, & Mayford M (1995) Impairment of spatial but not contextual memory in CaMKII mutant mice with a selective loss of hippocampal LTP in the range of the theta frequency. *Cell* 81(6):905-915.
17. Saghatelian A*, et al.* (2004) Assignment of endogenous substrates to enzymes by global metabolite profiling. *Biochemistry* 43(45):14332-14339.
18. Blankman JL, J.Z. L, Trauger SA, Siuzdak G, & Cravatt BF (2013) ABHD12 controls brain lysophosphatidylserine pathways that are deregulated in a murine

model of the neurodegenerative disease PHARC. *Proc Natl Acad Sci U S A* 110:1500-1505.
19. Tautenhahn R, Patti GJ, Rinehart D, & Siuzdak G (2012) XCMS Online: a web-based platform to process untargeted metabolomic data. *Analytical chemistry* 84(11):5035-5039.
20. Hsu FF & Turk J (1999) Structural characterization of triacylglycerols as lithiated adducts by electrospray ionization mass spectrometry using low-energy collisionally activated dissociation on a triple stage quadrupole instrument. *Journal of the American Society for Mass Spectrometry* 10(7):587-599.
21. Murphy RC*, et al.* (2007) Detection of the abundance of diacylglycerol and triacylglycerol molecular species in cells using neutral loss mass spectrometry. *Analytical biochemistry* 366(1):59-70.
22. Bachovchin DA*, et al.* (2010) Superfamily-wide portrait of serine hydrolase inhibition achieved by library-versus-library screening. *Proc Natl Acad Sci U S A* 107(49):20941-20946.
23. Hsu KL*, et al.* (2012) DAGLbeta inhibition perturbs a lipid network involved in macrophage inflammatory responses. *Nat Chem Biol* 8(12):999-1007.
24. Boersema PJ, Raijmakers R, Lemeer S, Mohammed S, & Heck AJ (2009) Multiplex peptide stable isotope dimethyl labeling for quantitative proteomics. *Nature protocols* 4(4):484-494.
25. Hulce JJ, Cognetta AB, Niphakis MJ, Tully SE, & Cravatt BF (2013) Proteome-wide mapping of cholesterol-interacting proteins in mammalian cells. *Nat Methods* 10(3):259-264.
26. Martin BR, Wang C, Adibekian A, Tully SE, & Cravatt BF (2012) Global profiling of dynamic protein palmitoylation. *Nat Methods* 9(1):84-89.
27. Washburn MP, Wolters D, & Yates JR, 3rd (2001) Large-scale analysis of the yeast proteome by multidimensional protein identification technology. *Nat Biotechnol* 19(3):242-247.
28. Weerapana E*, et al.* (2010) Quantitative reactivity profiling predicts functional cysteines in proteomes. *Nature* 468(7325):790-795.
29. Arrese EL, Patel RT, & Soulages JL (2006) The main triglyceride-lipase from the insect fat body is an active phospholipase A(1): identification and characterization. *J Lipid Res* 47(12):2656-2667.
30. Zimmermann R*, et al.* (2004) Fat mobilization in adipose tissue is promoted by adipose triglyceride lipase. *Science* 306(5700):1383-1386.
31. Hsu KL*, et al.* (2013) Development and optimization of piperidyl-1,2,3-triazole ureas as selective chemical probes of endocannabinoid biosynthesis. *J Med Chem* 56(21):8257-8269.
32. Wilson-Grady JT, Haas W, & Gygi SP (2013) Quantitative comparison of the fasted and re-fed mouse liver phosphoproteomes using lower pH reductive dimethylation. *Methods* 61(3):277-286.

Supporting Figures

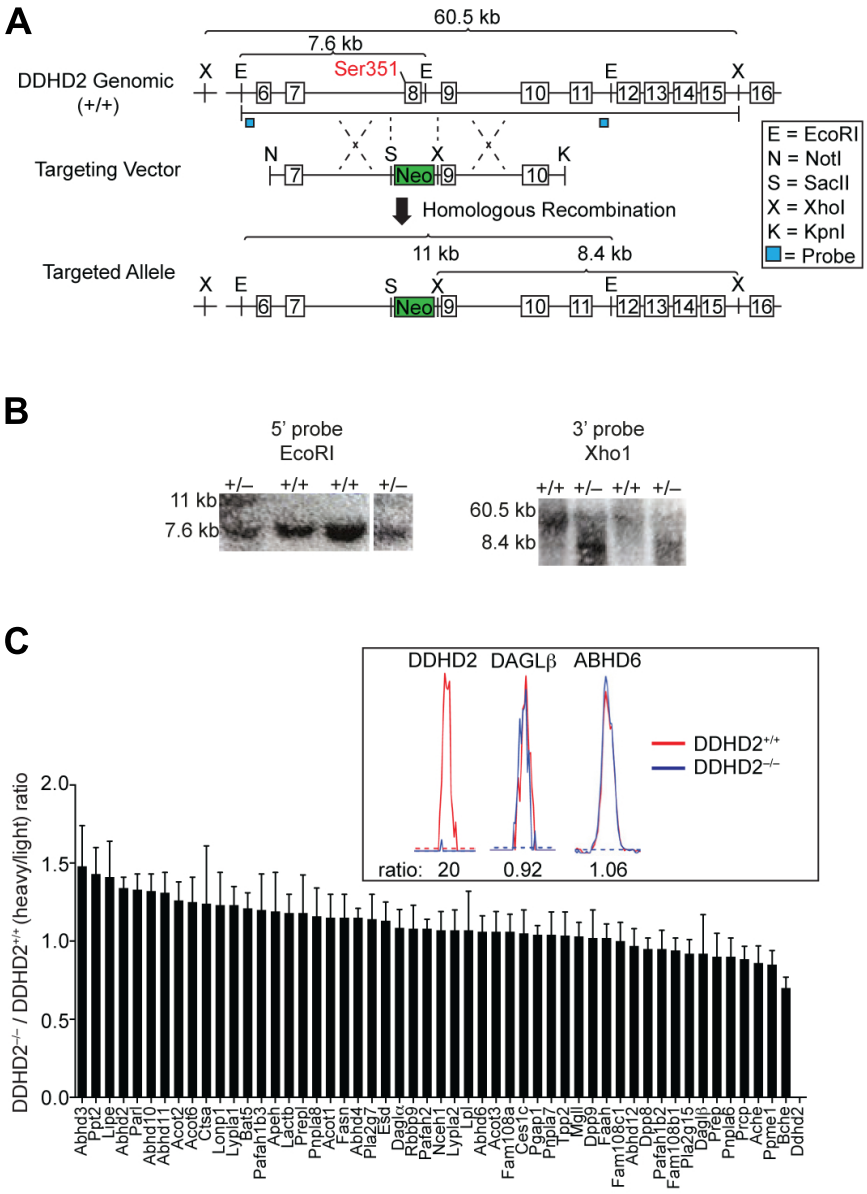

Fig. S1. Generation of mouse embryonic stem (ES) cells with a targeted disruption in the *Ddhd2* gene. (*A*) A gene-targeting vector was designed to replace *Ddhd2* exon 8 with a neomycin (Neo) selection cassette upon homologous recombination. (*B*) Southern blot analysis of EcoRI- or XhoI-digested embryonic stem cell genomic DNA was used to identify ES clones bearing targeted disruption of the *Ddhd2* gene (+/– cells) using 5' and 3' external probes, respectively. (*C*) Quantitative proteomics by ABPP-reductive dimethylation (see **Fig. S2** for more details on this method) confirmed selective absence of DDHD2 protein in DDHD2$^{-/-}$ brain tissue and no changes in other detected brain serine hydrolases in DDHD2$^{-/-}$ (heavy isotopically labeled) versus DDHD2$^{+/+}$ (light

isotopically labeled) brain proteomes. For bar graph, data shown are heavy/light ratios for the multiple peptides observed for each enzyme (average values ± standard error of a minimum of two unique peptides per enzyme) in combined soluble and membrane fractions from mouse brain tissue. Inset, parent-ion mass (MS1) traces for representative tryptic peptides from enriched serine hydrolases show absence of DDHD2, but not other serine hydrolase (DAGLβ, ABHD6) signals in DDHD2$^{-/-}$ mice. Data shown are from one experiment representative of two independent biological replicates.

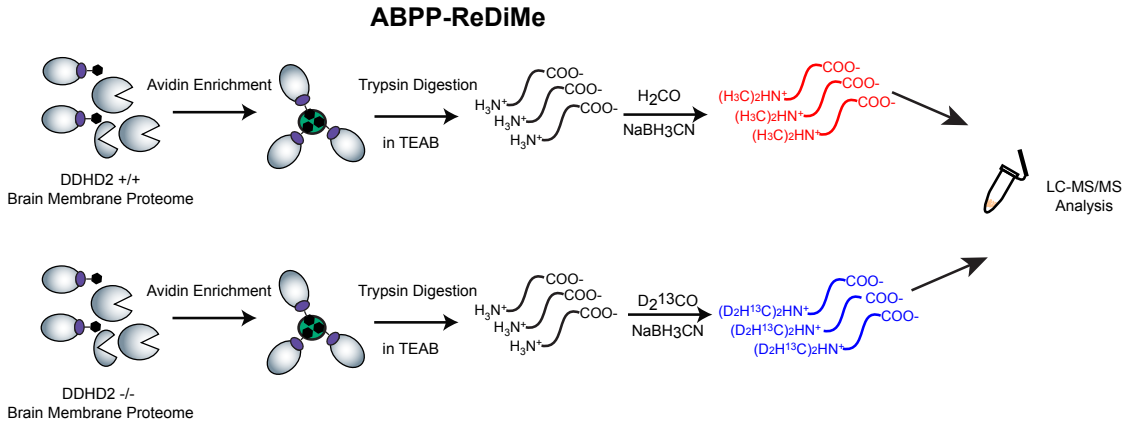

Fig. S2. Schematic of activity-based protein profiling-reductive dimethylation (ABPP-ReDiMe) method for quantifying serine hydrolase activities in mouse tissue proteomes. The fluorophosphonate (FP)-biotin probe used to label and enrich serine hydrolases is marked by a purple oval (FP)-black hexagon (biotin). For more details on MS methods for ABPP and reductive dimethylation, see (23) and (24, 32), respectively.

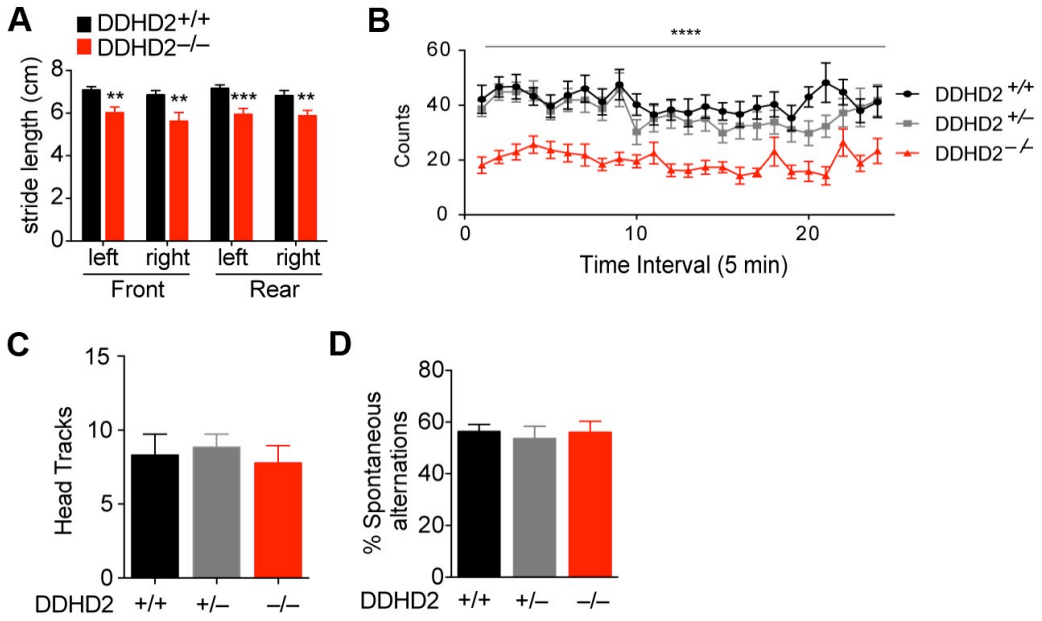

Fig. S3. DDHD2$^{-/-}$ mice have locomotor defects, but normal working memory. (*A*) Footprint pattern analysis uncovered shorter stride length in DDHD2$^{-/-}$ mice compared to DDHD2$^{+/+}$ mice. (*B*) DDHD2$^{-/-}$ mice exhibited a decrease in vertical movement (rearing) compared to DDHD2$^{+/+}$ and $^{+/-}$ mice. (*C*) DDHD2$^{+/+}$, DDHD2$^{+/-}$ and DDHD2$^{-/-}$ mice showed no differences in visual ability as measured by head tracking in the optomotor test. (*D*) In the Y-Maze test for working memory and exploratory behavior, similar spontaneous alternation frequencies were observed among genotypes. Data represent average values ± s.e.m.; n = 13 mice per group. $^{**}p < 0.01$, $^{***}p < 0.001$, $^{****}p < 0.0001$, for DDHD2$^{-/-}$ versus DDHD2$^{+/+}$ mice. Statistics in (*B)* performed using 2-way ANOVA with Fishers LSD across all time points.

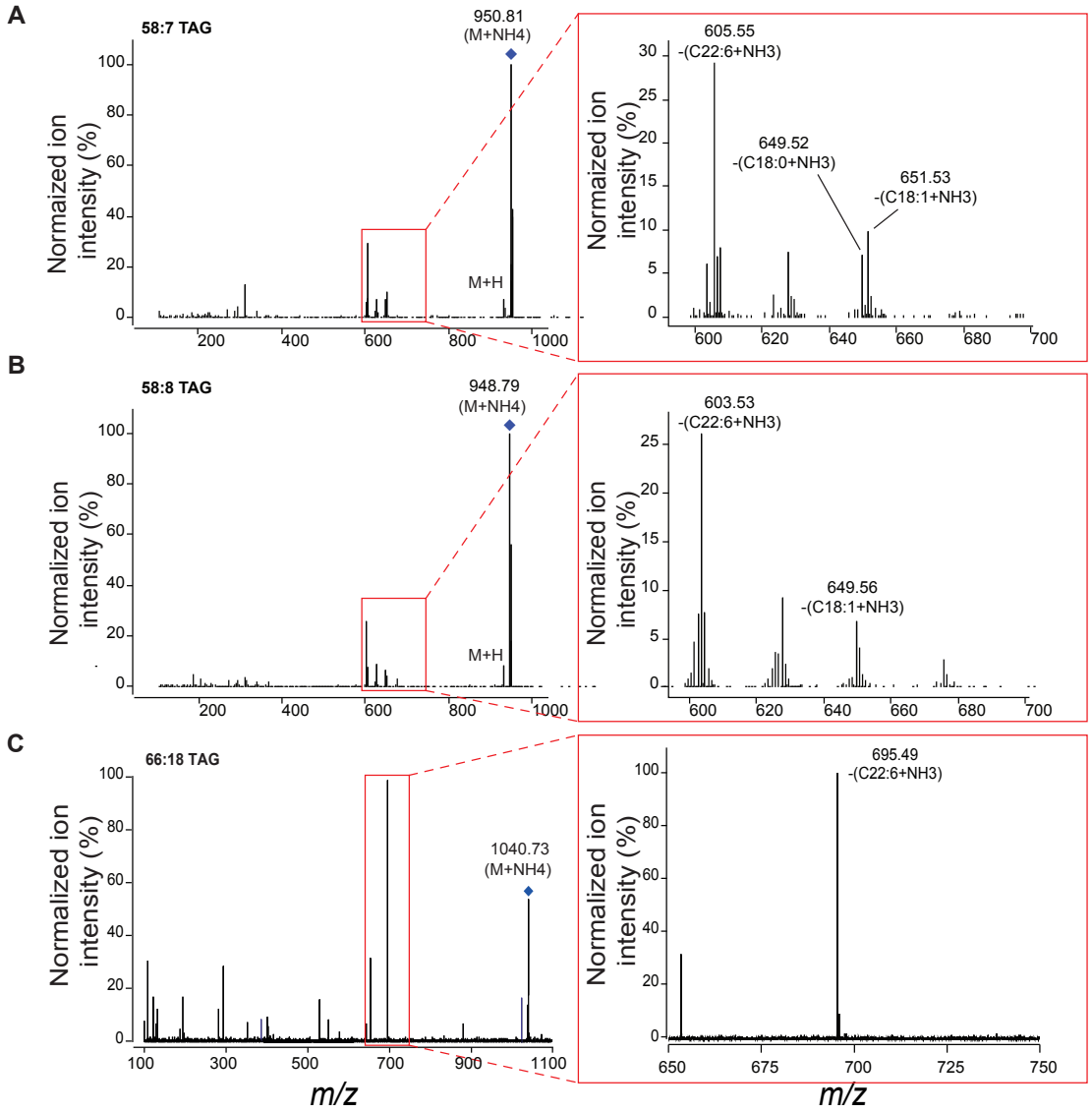

Fig. S4. Tandem MS analysis of DDHD2-regulated metabolites. Metabolites discovered by untargeted lipidomics to accumulate in brains of DDHD2$^{-/-}$ mice were subject to tandem MS analysis using an Agilent 6520 or Agilent 6538 Q-TOF (see Methods Section for more details). 950.8 (*A*), 948.8 (*B*), and 1040.8 (*C*) *m/z* species correspond to the (M+NH4) adducts of TAGs. Collision induced dissociation of species resulted in diagnostic DAG-like fragments (red box, zoom in right panels) that aided in structural assignments DDHD2-regulated metabolites. The composition of each TAG can be deduced by the neutral loss of each fatty acyl chain plus ammonia. The fragmentation pattern of 950.8, 948.8, and 1040.8 *m/z* species is consistent with C58:7, C58:8, and C66:18 TAG species, respectively.

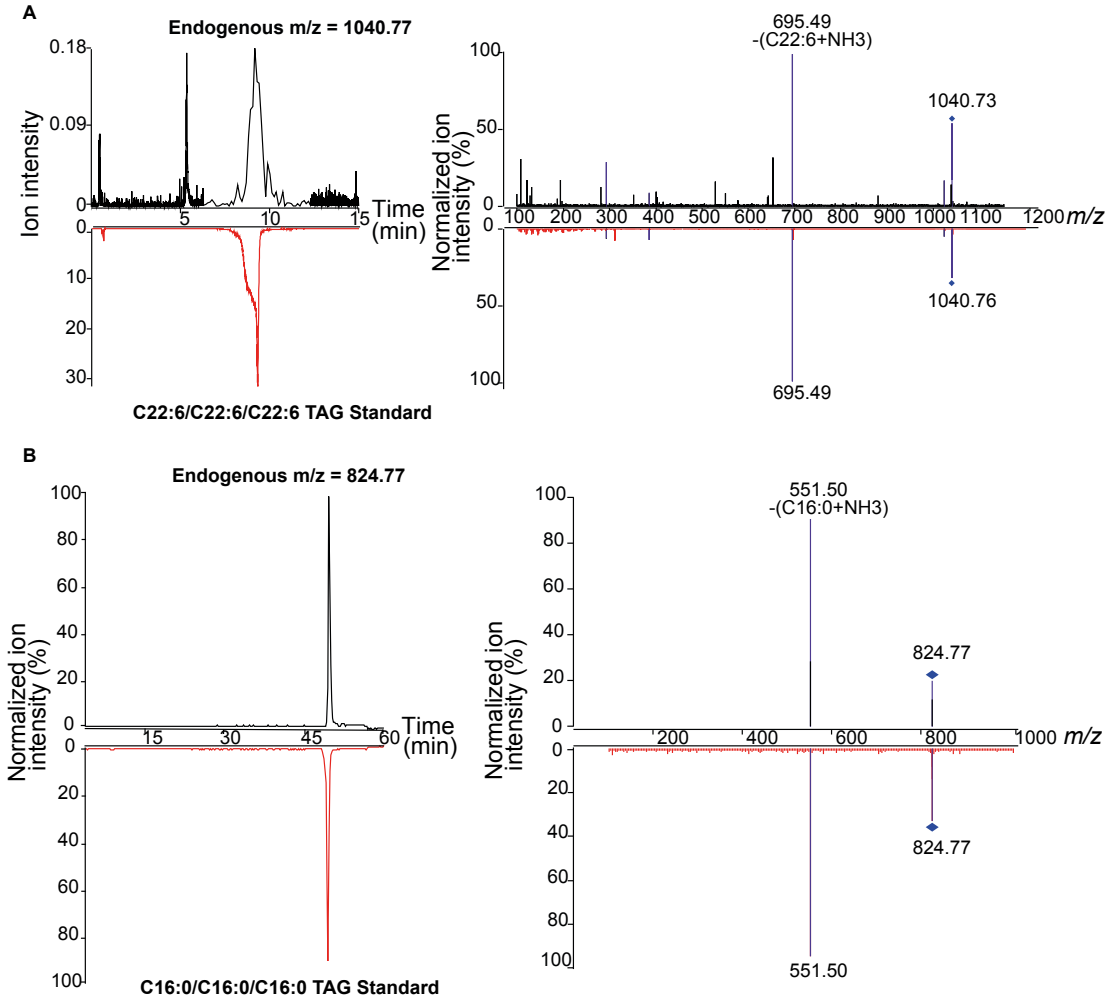

Fig. S5. Comparison of retention times and fragmentation spectra of DDHD2-regulated metabolites with lipid standards. Structural assignment of *m/z* 1040.8 (*A*) and 824.7 (*B*) *(m/z)* metabolites as C22:6/C22:6/C22:6 and C16:0/C16:0/C16:0 TAG species, respectively, based on matching retention times (left traces) and MS/MS fragmentation patterns (right traces) with commercially available synthetic standards. Tandem MS experiments were performed on an Agilent 6520 or Agilent 6538 Q-TOF (See Methods Section for more details).

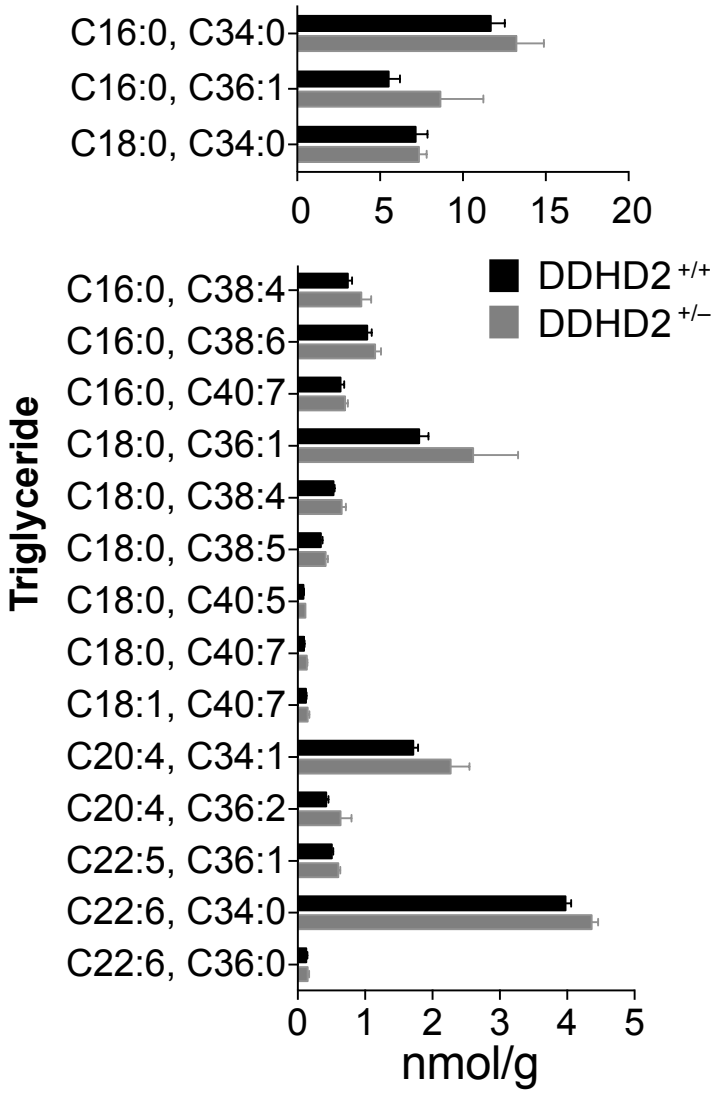

Fig. S6. Lack of TAG accumulation in brains of DDHD2$^{+/-}$ mice. Targeted LC-MS analysis of organic-soluble fractions from two-month old DDHD2$^{+/+}$ and DDHD2$^{+/-}$ brains. We did not observe significant accumulation of TAGs in DDHD2$^{+/-}$ brains. Data represent average values ± s.e.m.; n = 3 mice per group.

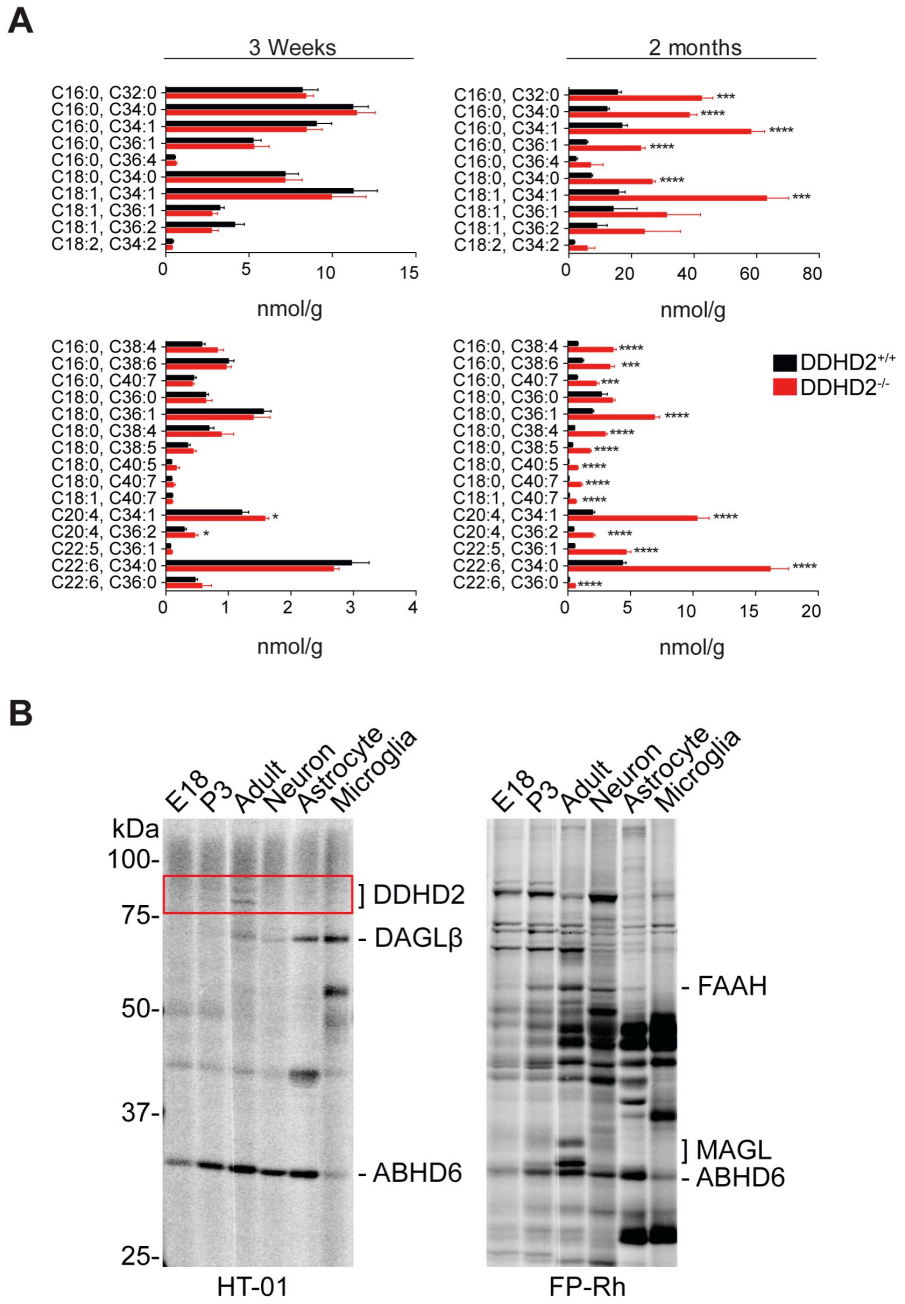

Fig. S7. Age-dependent expression of DDHD2 and TAG accumulation in DDHD2$^{-/-}$ mouse brains. *(A)* Targeted LC-MS analysis of organic-soluble fractions from DDHD2$^{+/+}$ and DDHD2$^{-/-}$ brains. TAGs showed limited accumulation in three-week old DDHD2$^{-/-}$ mice, but were significantly elevated by two-months of age. Data represent average values ± s.e.m.; n = 5 mice per group. *$p < 0.05$, ***$p < 0.001$, ***$p < 0.0001$ for DDHD2$^{-/-}$ versus DDHD2$^{+/+}$ mice. *(B)* Gel-based ABPP with the HT-01 probe (left, 1 μM, 30 min, 37 °C) or FP-Rh probe (right, 1 μM, 30 min, room temperature) of embryonic day 18 (E18), postnatal day 3 (P3), and adult (two months of age) mouse brain membrane proteomes, as well as of cultured neurons, astrocytes, and microglia. DDHD2 exhibits highest expression/activity in the mature brain and is detected at much lower levels (or not visible) during development or in isolated brain cells.

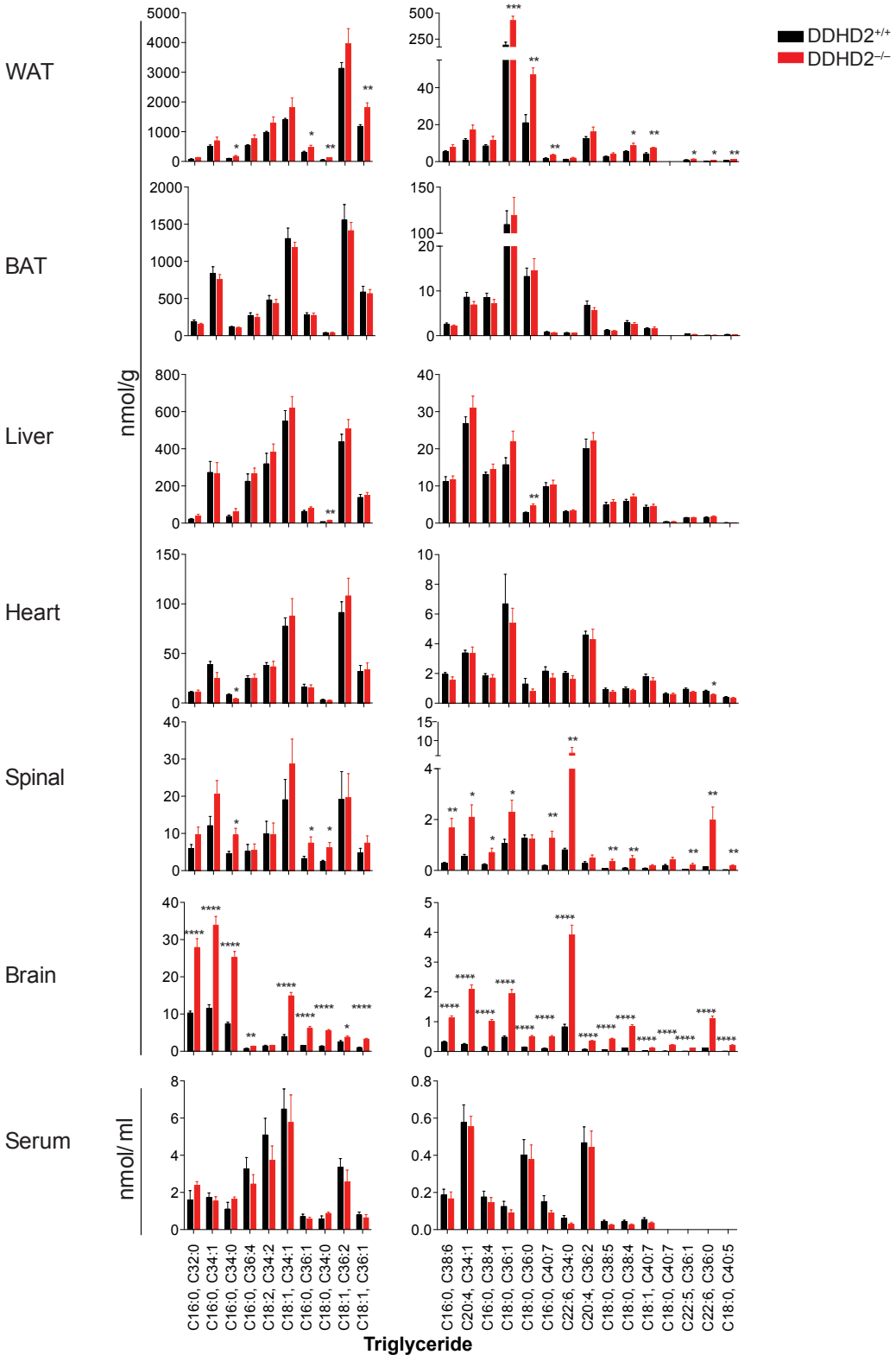
WAT
BAT
Liver
Heart
Spinal
Brain
Serum
nmol/g
nmol/ ml
DDHD2+/+
DDHD2−/−
C16:0, C32:0
C16:0, C34:1
C16:0, C34:0
C16:0, C36:4
C18:2, C34:2
C18:1, C34:1
C16:0, C36:1
C18:0, C34:0
C18:1, C36:2
C18:1, C36:1
C16:0, C38:6
C20:4, C34:1
C16:0, C38:4
C18:0, C36:1
C18:0, C36:0
C16:0, C40:7
C22:6, C34:0
C20:4, C36:2
C18:0, C38:5
C18:0, C38:4
C18:1, C40:7
C18:0, C40:7
C22:5, C36:1
C22:6, C36:0
C18:0, C40:5
Triglyceride

Fig. S8. TAG changes in DDHD2$^{-/-}$ mice are primarily observed in central nervous system tissue. Targeted LC-MS analysis of TAGs from 6-10 month old DDHD2$^{+/+}$ and DDHD2$^{-/-}$ mice. Substantial TAG accumulation occurred in the spinal cord and brain tissue of DDHD2$^{-/-}$ mice. Modest, but significant TAG accumulation was observed in white adipose tissue (WAT), but not in other peripheral tissues examined. Data represent average values ± s.e.m.; n = 5-9 mice per group. *$p < 0.05$, **$p < 0.01$, ***$p < 0.001$, ****$p < 0.0001$, for DDHD2$^{-/-}$ versus DDHD2$^{+/+}$ mice.

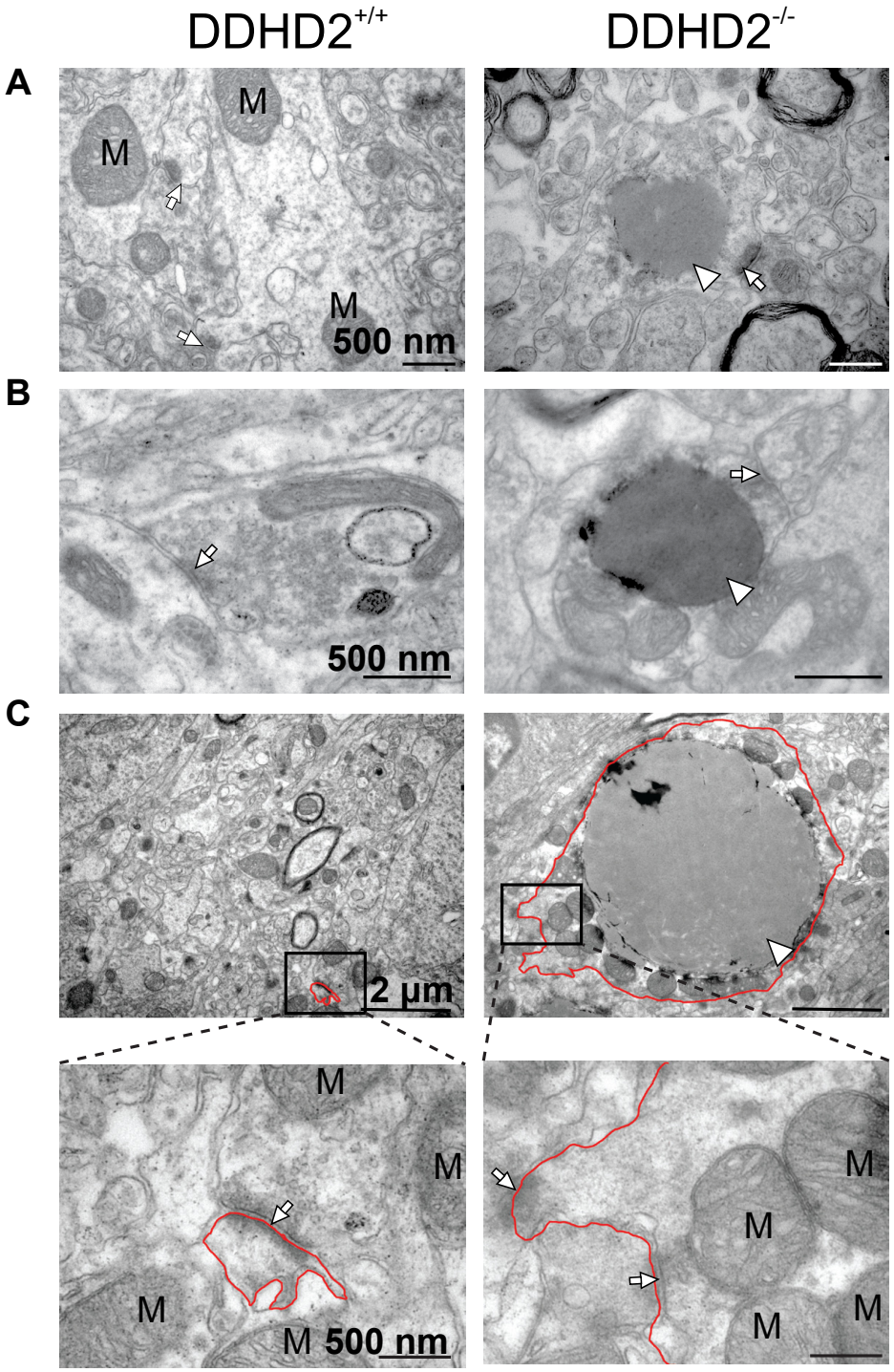

Fig. S9. Electron microscopy analysis of lipid droplets in three-month old DDHD2$^{-/-}$ mice. Large lipid droplets (LDs) were localized to dendrites in the postsynaptic region (*A*), as well as axons (*B*) of neurons in DDHD2$^{-/-}$ brains. The location of synapses onto the processes is illustrated. Dense staining of synaptic proteins and the presence of neurotransmitter containing vesicles mark axon termini. Foci of saturated electron density around the LDs in the DDHD2$^{-/-}$ axon are typical of this organelle. (*C*) Neuronal

processes in the DDHD2$^{-/-}$ brains contain large lipid droplets that likely cause swelling and displacement of mitochondria to the periphery. Insert shows magnification of synapses onto the process [(red line outlines margins of the process). M = Mitochondria, N = Nuclei, Arrows = synapses, Arrowheads = LD]. Scale bars: (*A*), (*B*) and bottom (*C*): 500 nm, top (*C*): 2 µm. Images shown are representative of 3 biological replicates per group.

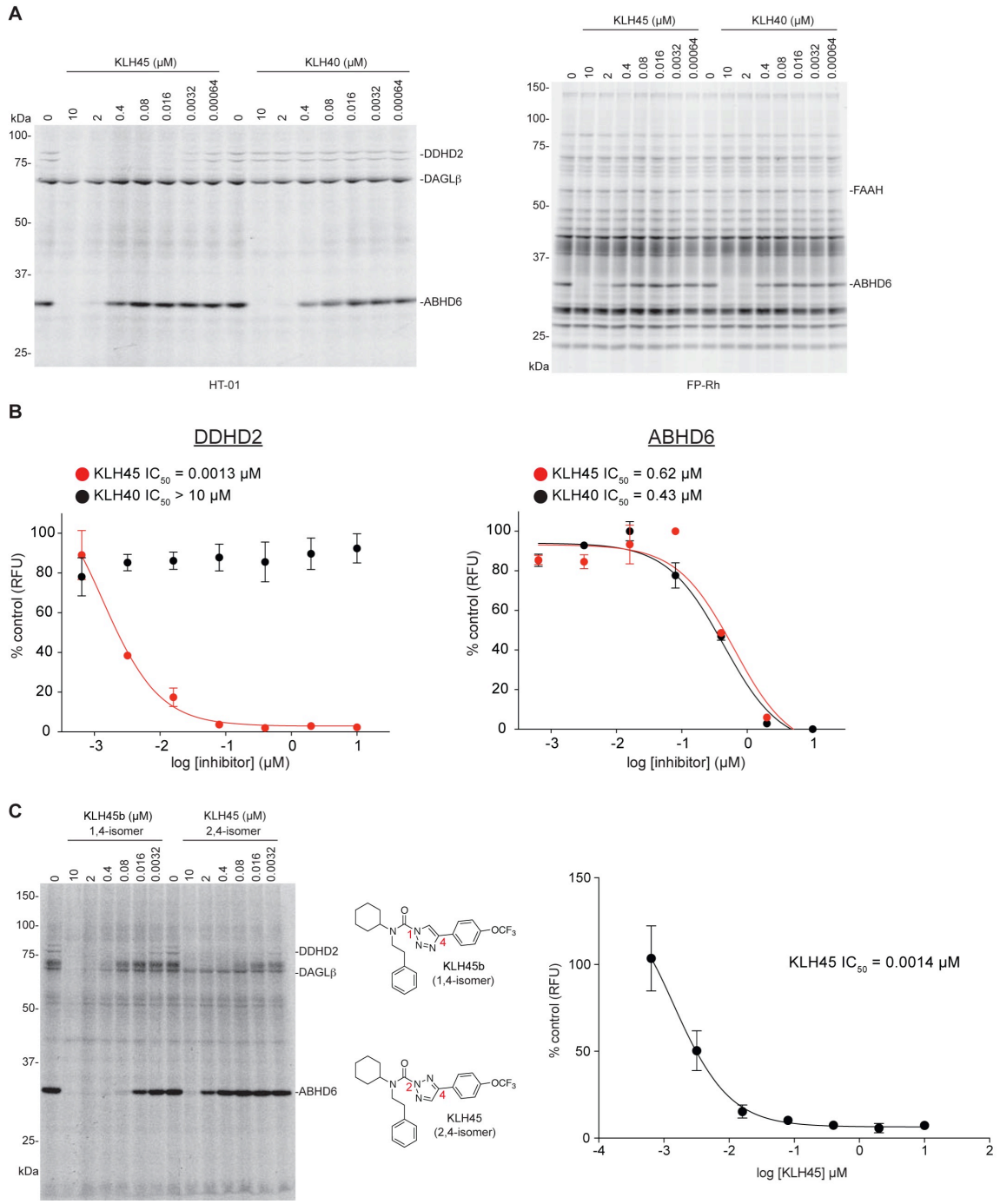

Fig. S10. Development of a potent and selective DDHD2 inhibitor KLH45 and a negative-control probe KLH40. (*A*) Inhibition of DDHD2 in Neuro2A membrane proteomes by KLH45, but not KLH40 as measured by the DDHD2-directed probe HT-01 (left gel) and general serine hydrolase probe FP-Rh (right gel). Note that KLH45 and KLH40 show similar activity against the single off-target ABHD6. (*B*) *In vitro* IC_{50} values for DDHD2 and ABHD6 inhibition by KLH45 and KLH40 as measured by competitive ABPP with the HT-01 probe. 95% confidence intervals for IC_{50} values: DDHD2-KLH45, 0.0006-0.003 μM; ABHD6-KLH45, 0.32-1.2 μM; ABHD6-KLH40, 0.27-0.69 μM. KLH40 showed negligible activity against DDHD2 across the entire dose range tested. Data

represent average values ± s.e.m. for 3 biological replicates. (*C*) Competitive ABPP of KLH45 and its 1,4-regioisomer (KLH45b) against serine hydrolases detected in mouse brain proteomes (DDHD2, DAGLβ, and ABHD6) using the HT-01 probe. Mouse brain membrane proteome (2 mg/mL) was incubated with varying concentrations of compounds for 30 min at 37 °C followed by labeling with HT-01 (1 μM, 30 min, 37 °C) and processing for analysis by gel-based ABPP. Inhibition of DDHD2 was detected by loss of HT-01 labeling. Data in right graph represent the IC50 value for the 2,4-regioisomer of KLH45 as an average value ± s.e.m. for two experimental replicates.

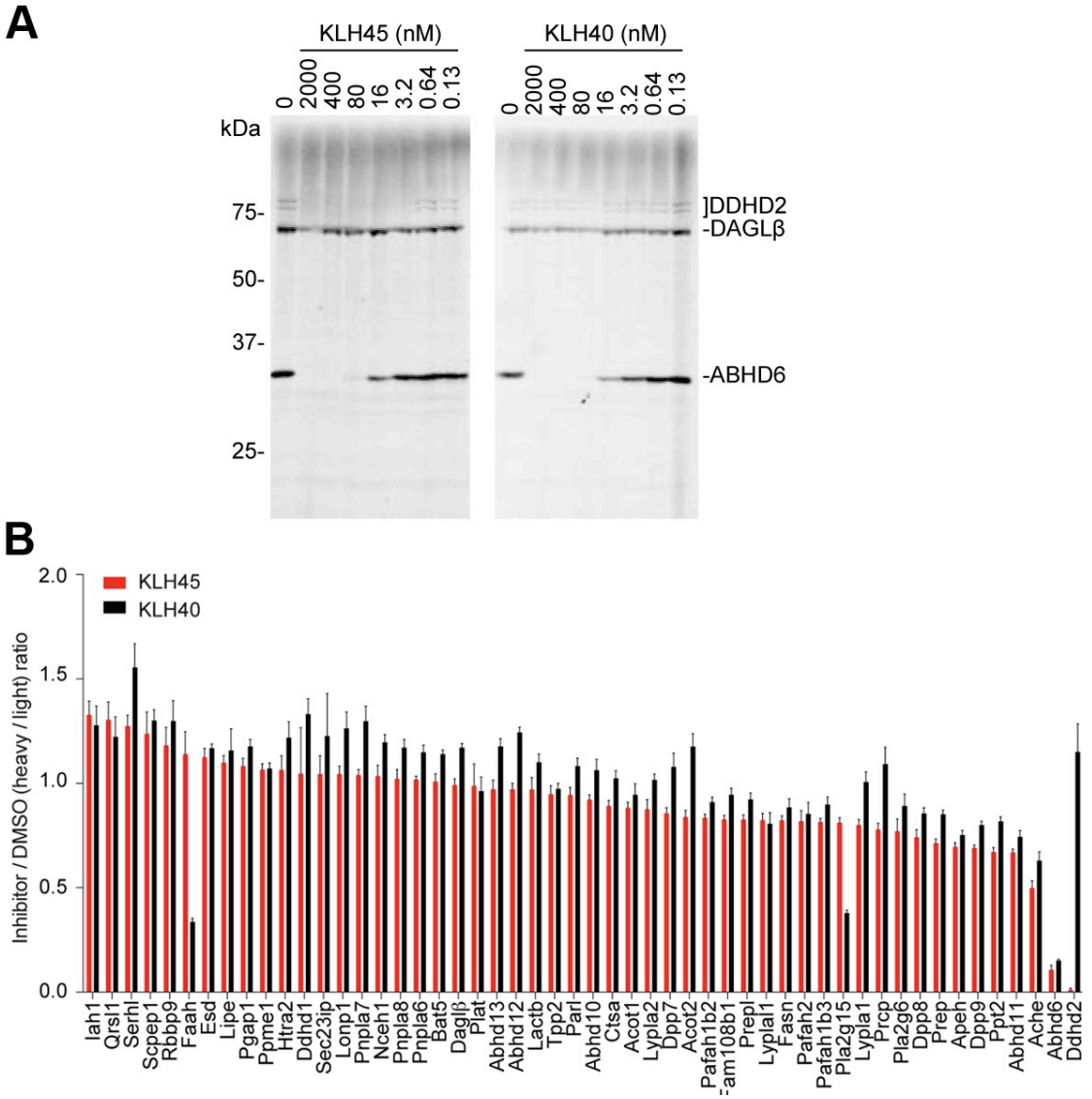

Fig. S11. *In situ* activity of KLH45 in Neuro2A cells. (*A*) Concentration-dependent inhibition of DDHD2 in Neuro2A cells by KLH45. In contrast, KLH40 showed negligible activity against DDHD2 in Neuro2A cells, but comparable cross-reactivity against ABHD6. Proteomes from treated cells (0.13 – 2000 nM compound, 4 h) were analyzed by competitive ABPP using the HT-01 probe (1 μM, 30 min, 37 °C). From these studies, we selected 25 nM as a suitable concentration of KLH45 (and the control probe KLH40) for ABPP-SILAC studies (*B*). ABPP gels shown are representative of two biological replicates. (*B*) ABPP-SILAC analysis showing that that KLH45 (25 nM, 4 h) inhibits DDHD2 with excellent selectivity in Neuro2A cells, exhibiting negligible cross-reactivity against the 50+ serine hydrolases detected in these cells with the exception of ABHD6, which is inhibited to a similar degree by the DDHD2-inactive control probe KLH40. Error bars represent mean ± s.e.m. of heavy/light ratios for multiple peptides detected for each enzyme (minimum of 3 unique peptides per enzyme) in combined soluble and membrane proteomes.

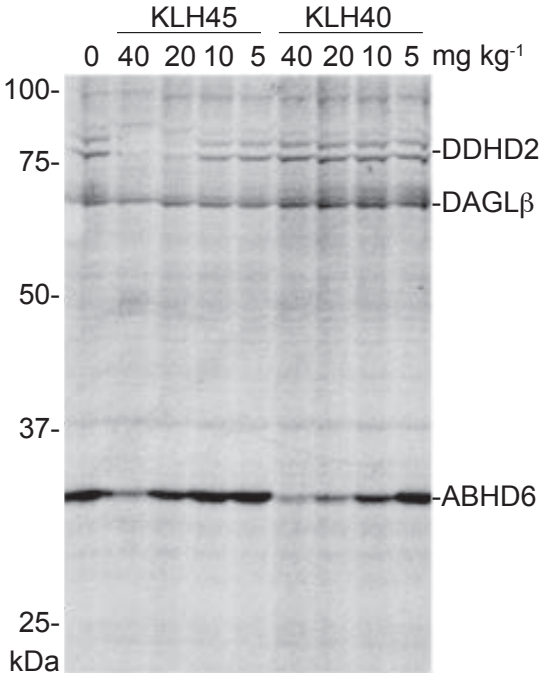

Fig. S12. Potency and selectivity of KLH45 and KLH40 *in vivo*. Dose-dependent inhibition of DDHD2 in brain proteomes from KLH45- or KLH40-treated mice (i.p., 4 hr) as measured by competitive ABPP using the HT-01 probe. At higher doses (40 and 20 mg per kg body weight), KLH45 treatment resulted in near-complete blockade of brain DDHD2 activity. In contrast, KLH40 showed no detectable cross-reactivity with DDHD2 at any tested dose. Both compounds inhibited ABHD6 in a dose-dependent manner. ABPP gels shown are representative of two biological replicates

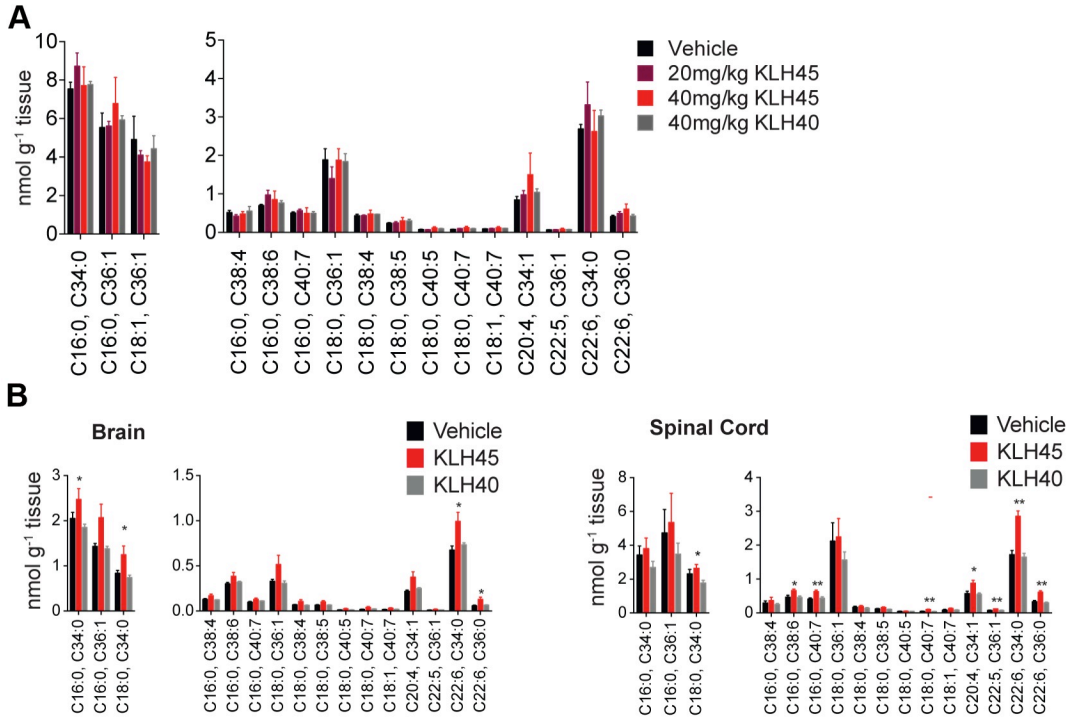

Fig. S13. Brain TAG measurements from mice treated acutely or subchronically with KLH45 or KLH40. (*A*) Mice were treated acutely with the indicated dose of compound for 4 h, sacrificed, and brain TAGs measured by targeted LC-MS analysis as described in the Methods section. We observed negligible accumulation of TAGs under these acute treatment conditions. Data represent average values ± s.e.m.; n = 3 mice per group. (*B*) Targeted LC-MS analysis revealed accumulation of TAGs in brain and spinal cord tissues from mice treated sub-chronically for four days with KLH45 versus vehicle or KLH40 (inhibitors were administered at 20 mg kg^{-1} compound, i.p., every 12 h). Data represent average values ± s.e.m.; n = 3-4 mice per group. *p <0.05, **p <0.01 for KLH40- versus KLH45-treated tissues.

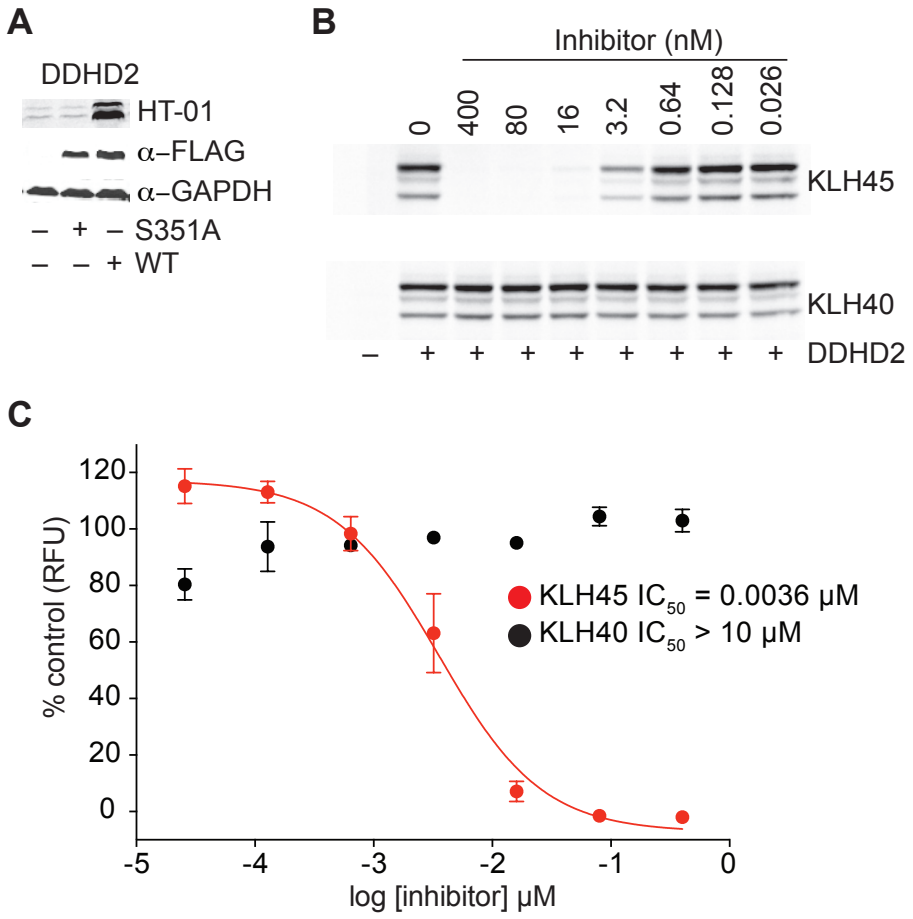

Fig. S14. Expression of recombinant DDHD2 in HEK293T cells. (*A*) Mouse DDHD2 wild-type (WT) and S351A mutant proteins were overexpressed at comparable levels as FLAG epitope-tagged fusion proteins in HEK293T cells by transient transfection (anti-FLAG antibody, 0.1 μg/mL; anti-GAPDH antibody, 0.167 μg/mL). WT-DDHD2, but not S351A-DDHD2 showed robust labeling by the HT-01 probe. (*B*) Concentration-dependent inhibition of recombinant DDHD2 in HEK293T proteomes by KLH45, but not KLH40 as measured by competitive ABPP with HT-01. (*C*) IC_{50} values for KLH45 and KLH40 against recombinant DDHD2 in HEK293T; data derived from gel-based competitive ABPP experiments. 95% confidence intervals for KLH45 IC_{50} value: 0.0022 - 0.0057 μM. Gel-based ABPP experiments were performed as described in **Fig. S10**. Data in part (*C*) represent average values ± s.e.m. for three experimental replicates.

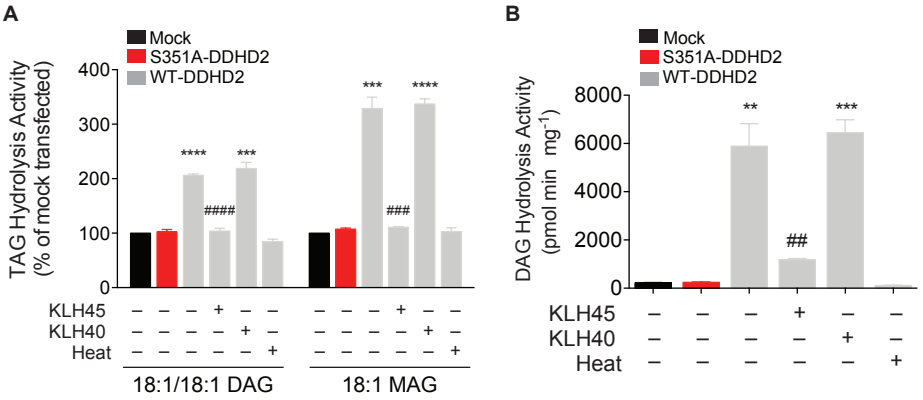

Fig. S15. Recombinant DDHD2 exhibits TAG and DAG hydrolase activities. WT-DDHD2-transfected HEK293T lysates, but not S351A-DDHD2-transfected lysates display enhanced TAG and DAG hydrolase activity relative to mock-transfected lysates. Substrate assays were conducted as described in the Methods section. Radiolabled TLC data shown in (*A*) was measured by monitoring conversion of ^{14}C-C18:1/C18:1/C18:1 TAG to ^{14}C-C18:1/C18:1 DAG or ^{14}C-C18:1 MAG (for measurements of ^{14}C-18:1 FFA see **Fig. 6a**). LC-MS data shown in (*B*) was measured by monitoring formation of C18:1 FFA product from C18:1/C18:1 DAG. Treatment with KLH45, but not KLH40 significantly blocked TAG and DAG hydrolase activity of DDHD2. Data represent average values ± s.e.m. for 3 biological replicates. $^{**}p$ <0.01, $^{***}p$<0.001, $^{****}p$<0.0001, for WT-DDHD2 or KLH40-treated WT-DDHD2 versus S351A-DDHD2 groups; $^{\#\#}p$ <0.01, $^{\#\#\#}$p<0.001, $^{\#\#\#\#}p$<0.0001, for KLH45-treated versus DMSO-treated WT-DDHD2 groups.

	M/Z	Ion	Retention Time (Minutes)	Fold Change (KO/WT)	P Value
MAG					
16:0	331.28	[M+H]+	38.74	0.85	0.32
18:0	359.32	[M+H]+	41.03	1.07	0.75
22:6	403.28	[M+H]+	37.80	0.95	0.71
DAG					
32:0	586.54	[M+NH4]+	47.71	1.08	0.30
34:1	612.56	[M+NH4]+	47.81	1.08	0.30
36:4	634.54	[M+NH4]+	47.39	1.05	0.56
36:3	636.56	[M+NH4]+	47.62	0.95	0.53
36:2	638.57	[M+NH4]+	47.90	1.08	0.41
36:1	640.59	[M+NH4]+	48.51	1.04	0.55
38:7	656.53	[M+NH4]+	46.69	0.99	0.33
38:6	658.54	[M+NH4]+	47.34	0.89	0.31
38:5	660.56	[M+NH4]+	47.48	0.93	0.63
38:4	662.57	[M+NH4]+	48.04	1.12	0.24
40:8	682.54	[M+NH4]+	45.39	1.15	0.52
40:7	684.56	[M+NH4]+	47.45	1.03	0.85
40:6	686.57	[M+NH4]+	48.00	1.22	0.04
42:6	706.54	[M+NH4]+	45.90	1.08	0.14
44:12	730.54	[M+NH4]+	45.44	1.16	0.41
44:11	732.56	[M+NH4]+	46.05	1.07	0.22
44:10	734.57	[M+NH4]+	46.89	1.05	0.25
TAG					
48:0	824.77	[M+NH4]+	57.66	2.07	<0.001
50:1	850.79	[M+NH4]+	57.97	2.72	<0.001
52:2	876.80	[M+NH4]+	58.28	2.70	<0.001
52:1	878.82	[M+NH4]+	58.29	2.70	<0.001
54:5	898.79	[M+NH4]+	55.95	2.76	<0.001
54:3	902.82	[M+NH4]+	58.40	2.43	0.02
54:0	908.86	[M+NH4]+	58.29	0.74	0.36
56:6	924.80	[M+NH4]+	58.26	2.25	0.01
58:8	948.80	[M+NH4]+	56.35	3.37	<0.001
58:7	950.82	[M+NH4]+	58.38	3.15	0.01
60:12	968.77	[M+NH4]+	53.72	2.26	<0.001
66:18	1040.77	[M+NH4]+	52.48	5.45	<0.001
66:15	1046.96	[M+NH4]+	51.03	0.83	0.32

	M/Z	Ion	Retention Time (Minutes)	Fold Change (KO/WT)	P Value
LPE					
16:0	454.29	[M+H]+	36.59	1.18	0.07
18:1	480.31	[M+H]+	36.75	0.96	0.79
18:0	482.32	[M+H]+	39.01	1.19	0.14
20:4	502.29	[M+H]+	35.48	1.05	0.77
LPC					
16:0	496.34	[M+H]+	36.65	1.15	0.11
18:1	522.36	[M+H]+	36.80	1.19	0.07
18:0	524.37	[M+H]+	39.16	1.08	0.54
20:4	544.34	[M+H]+	35.44	1.29	0.15
PE					
34:1	718.54	[M+H]+	46.80	1.09	0.23
36:4	740.52	[M+H]+	46.23	1.12	0.08
38:5	766.54	[M+H]+	46.43	0.99	0.83
38:4	768.55	[M+H]+	47.34	1.19	0.02
PC					
34:0	762.60	[M+H]+	48.16	1.01	0.91
36:1	789.62	[M+H]+	48.52	1.12	<0.001
FFA					
16:0	255.23	[M-H]-	33.92	0.96	0.81
18:1	281.25	[M-H]-	34.55	0.98	0.92
18:0	283.26	[M-H]-	36.42	1.06	0.62
20:4	303.23	[M-H]-	33.41	1.03	0.88
22:6	327.23	[M-H]-	33.60	0.73	0.24
22:0	339.33	[M-H]-	41.15	1.13	0.45
24:0	367.36	[M-H]-	43.23	1.16	0.44
LPA					
16:0	409.24	[M-H]-	32.13	0.95	0.72
18:1	435.25	[M-H]-	32.67	0.82	0.25
18:0	437.27	[M-H]-	34.78	0.89	0.57

	M/Z	Ion	Retention Time (Minutes)	Fold Change (KO/WT)	P Value
LPS					
16:0	496.27	[M-H]-	33.24	1.05	0.89
18:1	522.28	[M-H]-	33.58	0.98	0.91
18:0	524.30	[M-H]-	35.74	0.78	0.42
20:4	544.27	[M-H]-	32.29	1.04	0.86
22:6	568.27	[M-H]-	32.33	1.19	0.45
LPG					
20:4	531.27	[M-H]-	32.91	1.13	0.56
LPI					
16:0	571.29	[M-H]-	33.85	1.11	0.43
18:1	597.30	[M-H]-	34.37	1.07	0.60
18:0	599.32	[M-H]-	36.23	0.93	0.63
20:4	619.29	[M-H]-	32.70	1.44	0.24
22:6	643.29	[M-H]-	32.81	1.43	0.22
PA					
32:0	647.47	[M-H]-	45.89	1.08	0.35
34:1	673.48	[M-H]-	45.99	0.95	0.43
36:4	695.47	[M-H]-	45.08	1.01	0.89
36:2	699.50	[M-H]-	46.23	0.93	0.26
38:5	721.48	[M-H]-	45.51	1.34	0.25
38:4	723.50	[M-H]-	46.53	0.92	0.68
PS					
34:1	760.51	[M-H]-	45.20	1.07	0.64
36:2	786.53	[M-H]-	45.34	0.91	0.41
36:1	788.54	[M-H]-	46.46	1.02	0.86
38:4	810.53	[M-H]-	45.50	1.12	0.25
PG					
32:0	721.50	[M-H]-	45.16	0.79	0.03
34:1	747.52	[M-H]-	45.28	0.91	0.50
36:4	769.50	[M-H]-	44.72	1.02	0.90

Table S1. Untargeted lipidomics of brains from DDHD2$^{+/+}$ and DDHD2$^{-/-}$ mice. Representative group of phospholipids, lysophospholipids, free fatty acids, monoacylglycerols (MAGS), diacylglycerols (DAGs) and TAGS from DDHD2$^{+/+}$ and DDHD2$^{-/-}$ mice were quantified by manual integration. Fold changes are presented as the average integrated ion intensity in DDHD2$^{-/-}$ brains relative to DDHD2$^{+/+}$ brains. For a lipid to be considered significantly changed, it needed to show at least a two-fold difference in magnitude between DDHD2$^{+/+}$ and DDHD2$^{-/-}$ brains and a p value < 0.05. Based on these criteria, the only lipids that were observed to change in DDHD2$^{-/-}$ brains were TAGs (n = 6 mice per group). Internal lipid standards were quantified to account for differences in extraction efficiencies (fold-change for 15:0 FFA = 1.02, p = 0.95; 15:0 MAG = 1.07, p = 0.64). PE= phosphatidylethanolamine, LPE=lysoPE, PC=phosphatidylcholine, LPC=lysoPC, PA=phosphatidic acid, LPA=lysosPA, LPI; lysophosphatidylinositol, PS=phosphatidylserine, LPS; lysoPS, PG; phosphatidylglycerol, LPG=lysoPG.

Class	Species	Adduct	Precursor	Product	Colision Energy(V)
TAG	C17:1, C34:2	[M+NH4]+	860.7	575.5	15
TAG	C17:1, C34:0 d5	[M+NH4]+	869.8	584.6	15
TAG	C16:0, C32:0	[M+NH4]+	824.8	551.5	15
TAG	C16:0, C34:0	[M+NH4]+	852.8	579.5	15
TAG	C16:0, C34:1	[M+NH4]+	850.8	577.5	15
TAG	C16:0, C36:1	[M+NH4]+	878.8	605.6	15
TAG	C16:0, C36:4	[M+NH4]+	872.8	599.5	15
TAG	C16:0, C38:4	[M+NH4]+	900.8	627.5	15
TAG	C16:0, C38:6	[M+NH4]+	896.8	623.5	15
TAG	C16:0, C40:7	[M+NH4]+	922.8	649.5	15
TAG	C18:0, C34:0	[M+NH4]+	880.8	579.5	15
TAG	C18:0, C36:0	[M+NH4]+	908.8	607.6	15
TAG	C18:0, C36:1	[M+NH4]+	906.8	605.6	15
TAG	C18:0, C38:4	[M+NH4]+	928.8	627.5	15
TAG	C18:0, C38:5	[M+NH4]+	926.8	625.5	15
TAG	C18:0, C40:5	[M+NH4]+	954.8	653.6	15
TAG	C18:0, C40:7	[M+NH4]+	950.8	649.5	15
TAG	C18:1, C34:1	[M+NH4]+	876.8	577.5	15
TAG	C18:1, C36:1	[M+NH4]+	904.8	605.6	15
TAG	C18:1, C36:2	[M+NH4]+	902.8	603.5	15
TAG	C18:1, C40:7	[M+NH4]+	948.8	649.5	15
TAG	C18:2, C34:2	[M+NH4]+	872.8	575.5	15
TAG	C20:4, C34:1	[M+NH4]+	898.8	577.5	15
TAG	C20:4, C36:2	[M+NH4]+	924.8	603.5	15
TAG	C22:5, C36:1	[M+NH4]+	952.8	605.6	15
TAG	C22:6, C34:0	[M+NH4]+	924.8	579.5	15
TAG	C22:6, C36:0	[M+NH4]+	952.8	607.6	15

Table S2. List of multiple reaction monitoring (MRM) transitions used in targeted LC-MS experiments. Conditions to maximize signal of the targeted fragment ion were optimized on an Agilent 6460 QQQ. Unnatural lipid standards were targeted to standardize the signals of endogenous lipids.

Dataset S1. Complete proteomic data for ABPP-reductive dimethylation analysis of serine hydrolase activities in DDHD2$^{+/+}$ and DDHD2$^{-/-}$ brain tissues. Please see accompanying spreadsheet.

Dataset S2. Complete proteomic data for ABPP-SILAC analysis of serine hydrolase activities in KLH45- and KLH40-treated Neuro2A cells. Please see accompanying spreadsheet.